5. SITE 990[1]

Shipboard Scientific Party[2]

HOLE 990A

Date occupied: 20 September 1995

Date departed: 1 October 1995

Time on hole: 10 days, 17 hr, 15 min

Position: 63°28.372′N, 39°46.808′W

Bottom felt (drill-pipe measurement from the rig floor, m): 552.4

Distance between rig floor and sea level (m): 10.9

Water depth (drill-pipe measurement from sea level, m): 541.5

Total depth (from rig floor, m): 877.1

Penetration (m): 342.7

Number of cores (including cores having no recovery): 24

Total length of cored section (m): 160.7

Total core recovered (m): 105.0

Core recovery (%): 65.3

Oldest sediment cored:
Depth (mbsf): 202.3
Nature: conglomerate and volcaniclastic breccia
Earliest age: Eocene?

Top of basement:
Depth (mbsf): 211.9
Nature: basalt
Measured velocity (km/s): 2.8–6.2 (5.2 average)

Comments: Drilled from 0 to 182.0 mbsf. Recovered two pieces in Core 2M after reaming from 171.0 to 182.0 mbsf.

Principal results: Site 990 is located 52 km east of the East Greenland coast, within the southern drilling transect EG63, and is one of three drill sites planned to complete the stratigraphic sampling of the earliest volcanism along this margin. The site was located close to the position of previous ODP Site 915 to more deeply penetrate the lava succession and test the hypothesis that Iceland-type oceanic crustal accretion and steady-state production of Iceland-type tholeiites were initiated within this stratigraphic interval. Another important objective at the site was to sample material suitable for precise radiometric and magnetostratigraphic age determinations in order to assess the magnitude of a suspected hiatus in volcanic activity, located between the Lower/Middle Series lavas at Site 917 and the Site 917 Upper Series/Site 915 lavas.

Because the sedimentary section had been cored at Site 915 during Leg 152, Site 990 was washed to a depth of 182.0 m below seafloor (mbsf) and rotary cored below that level. Sediments recovered in the interval at 182.0–202.3 mbsf were subdivided into two lithologic units. According to ODP convention, these two units are termed lithologic Unit I and lithologic Unit II, even though data from Site 915 indicate that the material above 182 mbsf probably forms two additional lithologic units. As a result, we correlate lithologic Units I and II at Site 990 with lithologic Unit III at Site 915. The ages of both Site 990 units are unknown, but the ages of the overlying sediment and underlying basalt at Site 915 suggest an early Eocene age.

Lithologic Unit I is a calcite-cemented mixed-cobble conglomerate, dominated by clasts of altered basalt, gabbro, and dolerite; quartzite and siliciclastic siltstone form the remainder of the cobbles. The cobbles are generally rounded to well rounded and range in size from 4 to >12 cm in diameter. The matrix is a poorly sorted silty sand, with angular grains, sand-sized mudstone intraclasts, and calcite cement.

Lithologic Unit II directly overlies basalt and is a clayey volcaniclastic breccia, dominated by basaltic debris. Clasts in the breccia are predominantly angular and composed of dark yellowish brown, altered basaltic material. The matrix of the breccia is dominated by clay and iron oxides, probably derived from the alteration of basaltic material, and minor well-rounded silt to fine sand-sized quartz grains. The presence of poorly developed flow indicators, the repeated vertical changes between clast-supported and matrix-supported fabric, and the absence of macroscopic pedogenic features indicate that Unit II was deposited as a mass flow, such as a matrix-rich debris flow, after a limited transport distance. The large size and the rounding of the clasts in lithologic Unit I suggest that this unit was deposited in a high-energy environment, possibly a high-gradient stream; a shallow, wave-influenced marine setting; or a fan delta.

Additional sedimentary material, apparently untransported, was recognized as red, brecciated to clayey material on the top of flow units within the basalt basement. This material has been described as part of the igneous sequence, but reflects in situ alteration and soil development.

Thirteen igneous flow units were recognized in the core recovered from the interval 211.9–342.7 mbsf, on the basis of changes in phenocryst assemblage or the presence of weathered and/or vesicular flow tops. Lava flows fall into one of three types: aa, pahoehoe, and transitional. Pahoehoe flows dominate in the lower part of the drilled sequence, whereas aa flows are ubiquitous in the upper portion. The top of the volcanic section at this site (and at previously drilled Site 915) is deeply weathered and oxidized, indicating that eruption occurred subaerially with some time gap between successive flow units.

The flow units cored at Site 990 range from aphyric to highly olivine or plagioclase-olivine-clinopyroxene phyric basalt. The olivine content decreases upward in the section, whereas both grain size and flow thickness increase upward. There is a subtle but systematic compositional variation in trace-element contents from the base to the top of the sequence (i.e., decreasing Cr and Ni and increasing V, Nb, Zr, and Y). In general, the lavas are moderately evolved, with low trace-element abundances, and geochemically similar to the one unit recovered from nearby Site 915 and all units at Site 918 (72 km to the southeast). No lavas similar to the Upper Series units cored at Site 917 (3 km to the west) were found, indicating that the transition from the breakup-related series to the Iceland-type

[1]Duncan, R.A., Larsen, H.C., Allan, J.F., et al., 1996. *Proc. ODP, Init. Repts.*, 163: College Station, TX (Ocean Drilling Program).
[2]Shipboard Scientific Party is given in the list preceding the Table of Contents.

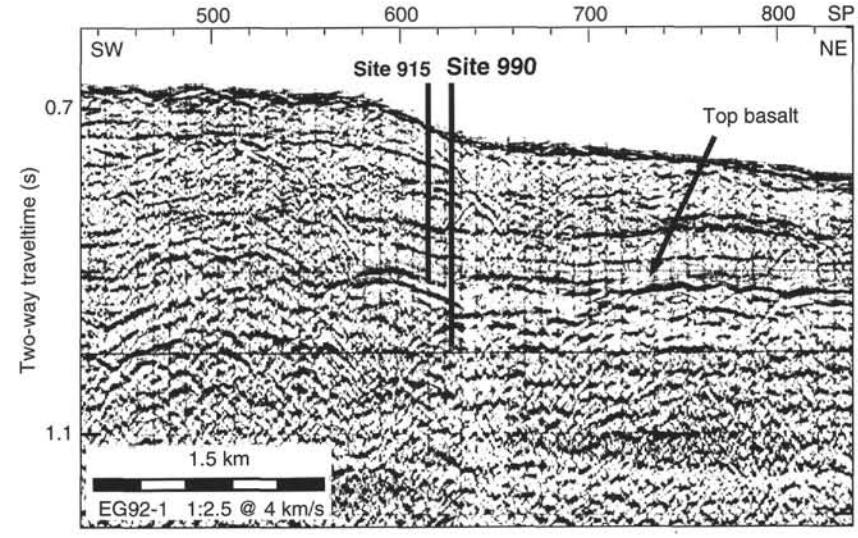

Figure 1. Seismic cross section through Site 990 (strike line). See Figures 1 and 2, "Site 989" chapter (this volume), for the location and seismic dip line. ODP Site 915 is described in Larsen, Saunders, Clift, et al. (1994).

tholeiitic series that dominates the oceanic seaward-dipping reflector sequence is abrupt and occurs over a stratigraphic interval of <100 m.

The basaltic rocks recovered at Site 990 exhibit numerous planar, primary magmatic features that consist of vesicular layers, elongated patches of filled vesicles, and widely developed diffuse, thin flow bands. Many of these magmatic features occur in an almost horizontal attitude. The only evidence of deformation consists of a relatively dense network of veins and, to a lesser extent, of fractures, some of which show the development of slickensides. The veins, usually 1–2 mm thick, are commonly lined and filled with green clay. Other minerals less commonly seen in veins include zeolite minerals, carbonates, native copper, and gypsum.

Paleomagnetic data for the Site 990 basalts reveal a magnetic reversal between the upper two normally magnetized flows and the lower 11 reversely magnetized flows. Integration with the Leg 152 results suggests that the normal polarity interval may be correlated with either Chron C25n or C26n and the underlying reverse polarity interval with C25r or C26r. The discovery of normal polarity intervals, together with future radiometric dating, offers the promise of a precise chronology for East Greenland margin volcanism.

Measurements of index properties from split core sections and discrete minicores correlate with flow structure. Specifically, *P*-wave velocities and bulk densities vary respectively from 2 km/s and 2.3 g/cm^3 in altered, vesicular flow tops to 6 km/s and 3.0 g/cm^3 within the central, more compact portions. From the high rates of recovery and detailed sampling, it is apparent that the often reported differences between velocity and density measurements on discrete core and estimates derived from seismic reflection or downhole logging result from preferential recovery of the compact, central flow material. Magnetic susceptibilities range from 100×10^{-5} SI to 5000×10^{-5} SI. Thermal conductivity values are similar to those measured at Hole 989B, namely ~2 $Wm^{-1}K^{-1}$.

BACKGROUND AND OBJECTIVES

Site 990 is located approximately 52 km offshore of the East Greenland coast, within the southern drilling transect EG63 (Fig. 1), and is one of the three drill sites planned for this transect (Fig. 3, "Introduction" chapter, this volume). Site 915 is located within the seaward part of the mid-shelf flexure zone where lavas of the SDRS onlap the basement and dip seaward below a cover of postvolcanic sediments (Fig. 1; see also "Background and Objectives" section, "Site 989" chapter, this volume). Site 990 is offset 8 km in the down-dip direction (southeast) from Site 989 and 3 and 2 km from Sites 917 and 916, respectively. Site 990 was planned to expand the basement penetration of Site 915 and is located about 150 m northeast of that site. Sites 915–917 were drilled during Leg 152 (Larsen, Saunders, Clift, et al., 1994).

The five sites (Sites 989, 917, 916, 915, and 990) provide a detailed stratigraphic sampling of the earliest volcanism along the EG63 transect. The lavas drilled at Sites 917 and 915 record a development from initial continental volcanism (Lower and Middle Series lavas) through transient picritic volcanism and into oceanic volcanism (Upper Series and younger lavas; see Fig. 2, "Site 989" chapter, this volume). The Upper Series lavas at Site 917 are more depleted and less affected by contamination with continental crust than the earlier units. The only igneous unit cored at Site 915 exhibited a more Iceland-type tholeiitic composition and a further reduction in continental contamination (Fitton et al., in press). Hence, the development of Iceland-type oceanic crustal accretion is interpreted to take place within the stratigraphic interval between the top of Site 917 and Site 915.

The lavas from Sites 917 and 915 show a reverse magnetic polarity (Larsen, Saunders, Clift, et al., 1994). The age of the reversely magnetized Lower and Middle Series (Larsen, Saunders, Clift, et al., 1994) has been established radiometrically at about 61 Ma (Sinton et al., 1994; Sinton and Duncan, in press), suggesting a correlation with magnetic Chron C26r or C27r. Because of alteration and low K contents, it has not been possible to date the Upper Series lavas or the Site 915 lava with any reliability. Site 915 is located within the oldest, landward part of the main SDRS (thought to be of C24r age, 53–56 Ma; Berggren et al., 1995; see also "Introduction" chapter, this volume). However, the site is also close to the transition from the Middle Series to the Upper Series. Hence, a significant hiatus (61 to 56 Ma) may be present between the Middle and Upper Series, or alternatively, the Site 915 lavas may be significantly older than Chron C24r (>56 Ma).

Site 990 is located at a water depth of 541.5 m (Figs. 1, 2, "Site 989" chapter, this volume, and Fig. 1). The lava sequence dips gently seaward at approximately 10°–15° and shows the typical stratigraphic pattern of the SDRS complex: increasing dip with depth and therefore a downward divergence of the stratigraphic units. The location of Sites 915/990 is the most landward position where this typical SDRS structure is imaged. The top of the lava pile around Sites 915/990 is a smooth surface in the dip direction (Fig. 2, "Site 989" chapter, this volume), but the cross line along strike of the dipping lava sequence shows some irregularities (Fig. 1), possibly resulting from erosion or a primary depositional relief.

The main objective of drilling at Site 990 was to penetrate deeper into the lava succession than at Site 915 in order to test the hypothesis that Iceland-type oceanic crustal accretion and steady-state produc-

tion of Iceland-type tholeiites was initiated within this stratigraphic interval. Another important objective at the site was to sample material suitable for precise age determination by $^{40}Ar/^{39}Ar$ and magnetostratigraphic methods from the older part of the SDRS, but above the already dated Lower and Middle Series of Site 917. The age of this interval is needed to determine the magnitude of the hiatus between the Middle and Upper Series and thereby to constrain the time interval in which the main SDRS formed (see also "Introduction" chapter, this volume; Larsen, Saunders, Clift, et al., 1994). The timing and duration of these events are critical to understanding and modeling the progressive thinning of the continental lithosphere and in estimating the rate of spreading and magmatic productivity during the main phase of SDRS formation.

At Site 915, 85 m of glaciomarine sediments and 104 m of upper Eocene shelf sediments, middle Eocene shallow-marine sediments, and a basal conglomerate (Eocene?) were cored before volcanic basement was reached at 189 mbsf. Site 990 was planned to be wash drilled to 180 mbsf and then RCB cored.

OPERATIONS

The site beacon was dropped by Global Positioning System coordinates at 2145 UTC on 20 September, after dynamically moving the vessel from Site 989. A standard nine-collar RCB bottom-hole assembly (BHA) was made up with a C-4 bit and a mechanical bit release (MBR). Because the sediment section of this site had been cored on Leg 152, the plan was to drill through most (180 m) of the sediments and core from this depth into basement.

Reentry

The hole was drilled to 41 mbsf before excessive heave generated by a sudden gale forced us to come out of the hole for 3 hr. We reentered the hole at 0645 UTC on 21 September and advanced to 27 mbsf before drilling was stopped again to allow a large iceberg to clear the drilling area.

A free-fall funnel was then deployed to ensure that any progress would not be lost if a sudden exit were required because of ice or weather. Drilling resumed and the hole was deepened to 45 mbsf when another iceberg approached, forcing the driller to lift the bit to 10 mbsf. The 70-m-high iceberg passed within 1.9 km of the vessel, moving south at 1.1 kt. Two more hours of washing and reaming were required before advancing the bit back down to 45 mbsf.

By 0515 UTC on September 22, the hole had been deepened to 63 mbsf. At this time, the mates on the bridge suddenly detected a large bergy bit very close to the vessel. The drill floor was advised to pull out of the hole and the vessel was immediately offset to starboard. A second growler was then observed within 10 m of the vessel. The ship changed heading to meet this piece of ice head on, and it bounced off the port bow and then passed the vessel on the port side, without causing damage. The low profile of the ice, combined with the rough sea state, made it difficult to detect growlers and bergy bits by radar or with searchlights.

After waiting on ice for 15 min, the bit was pulled to the surface and a mill-tooth tricone drilling bit was made up with an MBR. It was expected that the mill-tooth bit would penetrate the 180 m of sediment much faster than a coring bit.

Second Reentry

The second reentry of the hole was accomplished at 1530 UTC on 22 September. The hole was washed and reamed from 10 to 134 mbsf, after which the hole was drilled ahead to 182 mbsf. After flushing the hole with mud, the bit was tripped to the surface to change to a coring bit.

Third Reentry

A new C-4 bit was made up with a nine-collar BHA and run back to the bottom of the hole, and at 0322 UTC on 24 September, the third reentry of the hole was made. The hole was washed and reamed from 19 to 181 mbsf, after which the wash barrel was retrieved and a core barrel dropped. Finally, at 0900 UTC, coring was initiated in Hole 990A (Table 1). After a first core containing conglomerate and drilling rubble was retrieved, coring had to be terminated because of a developing storm. The drill string was pulled out of the hole, with the bit clearing the seafloor at 1600 UTC that day. A Force 10 storm from the north prevailed during the afternoon and late into the evening, with wind gusts as high as 60 kt and 20–30-ft seas.

By 1100 UTC the next day, the winds had died down and the large swell was abating. Reentry of the hole was delayed for nearly 5 hr to repair the defective video camera on the vibration-isolated television system.

Medical Evacuation

During this storm, a lost-time accident occurred involving crane operator Andy Fitzmorris. One half of a free-fall funnel was secured to the starboard main deck under the drill floor with new $^{3}/_{8}$-in. cargo chain. A large wave came over the side, hit the free-fall funnel half, broke the chain, and washed the funnel half into the aft moonpool tugger. Andy and two other men were trying to resecure the funnel half when another wave came over the side. Andy was hit by the wave and lost his footing while holding on to the chain to avoid being swept into the moonpool, which resulted in a dislocated shoulder with torn ligaments. A medivac helicopter arrived the next day (25 September) at 1505 UTC and transported Andy to Ammassalik, Greenland, from where he was flown to Iceland.

Fourth Reentry

At 1700 UTC on 25 September, the hole was reentered, and after extensive reaming of the bottom section (181–191 mbsf), coring was resumed in Hole 990A. Rotary coring advanced routinely to 260 mbsf, where the drill pipe got stuck. After the string was picked up to 249.6 mbsf to retrieve Core 163-990A-12R, the hole began to pack off around the drill string and circulation and rotation were lost. After restoring rotation and working the pipe up the hole for 2.5 hr (incurring overpulls as large as 200,000 lb, with a 420,000-lb total string weight), the drill string finally became free. Because of the presence of a large iceberg approaching the location, the bit was then tripped to the surface for inspection. Although the bit was in good condition, drilling resumed with a new C-4 bit and new MBR.

Fifth Reentry

At 2100 UTC on 27 September, iceberg number 107 of the leg passed within 0.9 km of the vessel, moving south at 1.2 kt. The first mate calculated the height of the iceberg using radar distance and sextant angle to be 135 m. The captain then gave approval to reenter the hole, with the bit reentering the free-fall funnel at 2115 UTC.

The bit was run into the hole to 166 mbsf without reaming, indicating that the top portion of the hole was now stabilized. The hole was washed and reamed from 166 to 231 mbsf and then flushed with a high-viscosity mud. The bit was subsequently run back into the hole

Table 1. Site 990 coring summary.

Core	Date (Sept. 1995)	Time (UTC)	Depth (mbsf)	Length cored (m)	Length recovered (m)	Recovery (%)
163-990A-			***Drilled from 0.0 to 182.0 mbsf ***			
1R	24	1115	182.0–191.6	9.6	1.66	17.3
2M	24	1800	171.0–191.0	0.0[a]	0.13	
3R	26	0210	191.6–202.3	10.7	5.51	51.5
4R	26	0800	202.3–211.9	9.6	0.00	0.0
5R	26	1130	211.9–217.4	5.5	4.93	89.6
6R	26	1400	217.4–221.4	4.0	5.16	129.0
7R	26	1730	221.4–231.1	9.7	5.26	54.2
8R	26	1930	231.1–240.7	9.6	5.36	55.8
9R	26	2215	240.7–245.7	5.0	4.14	82.8
10R	27	0205	245.7–250.3	4.6	6.59	143.0
11R	27	0625	250.3–255.0	4.7	2.16	45.9
12R	27	0915	255.0–260.0	5.0	1.69	33.8
13R	28	0640	260.0–264.6	4.6	4.40	95.6
14R	28	0950	264.6–269.6	5.0	3.68	73.6
15R	28	1400	269.6–275.3	5.7	5.42	95.1
16R	28	1550	275.3–279.3	4.0	4.36	109.0
17R	28	1900	279.3–288.9	9.6	6.80	70.8
18R	28	2205	288.9–298.6	9.7	7.27	74.9
19R	29	0030	298.6–304.2	5.6	6.03	107.0
20R	29	0305	304.2–308.2	4.0	4.25	106.0
21R	29	0600	308.2–317.9	9.7	5.35	55.1
22R	29	0800	317.9–327.5	9.6	7.00	72.9
23R	29	1010	327.5–337.1	9.6	5.40	56.2
24R	29	1215	337.1–342.7	5.6	2.46	43.9
Coring totals:				160.7	105.01	65.3
Drilled:				182.0		
Total:				342.7		

[a]Reaming never got back to bottom (191.0 mbsf) but recovered two pieces in Core 163-990A-2M.

to 260 mbsf, where coring was resumed. Rotary coring advanced in basalt from 260.0 to 302.7 mbsf, with increasing rates of penetration and excellent recovery. Within this interval, the average rate of penetration was 3.1 m/hr (with rates as high as 4.8 m/hr) with an average recovery of 85.9%. As coring advanced from 302.7 to 343.1 mbsf, the rate of penetration increased significantly and recovery dropped (44%–56%), with an extraordinarily high rate of penetration (7.2 m/hr) from 317.9 to 327.5 mbsf.

By 1200 UTC on 29 September, the winds had increased to 40 kt, with gusts to 50 kt from the north and 18-ft seas. The sea state was complex, with swells coming from the north and east. The vessel heave increased to 16–18 ft, with very short period excursions. As a result, rapid and confused ship motion developed, which caused the heave compensator to bottom out. Coring operations were stopped and the pipe pulled out of the hole to 144 m below sea level to wait for the storm to blow over.

The Storm

From the Danish Meteorological Institute (DMI) weather forecast of 28 September, we expected gale force winds from the northeast, starting on the morning of 29 September and extending into the morning of 1 October. The maximum sustained winds were forecast to be 23 m/s (approximately 47 kt).

During the morning of 29 September, the winds increased gradually from the north to a sustained 42 kt with gusts to 50 kt by noon. The winds then began to slowly shift to the north-northeast and decreased to 20 kt by 1800 UTC. The winds then started to increase, with the direction holding steady from the north-northeast. When the DMI evening forecast arrived 2130 UTC, the wind forecast had been revised upward in strength to 50–60 kt from the north-northeast to north for the next 48 hr, indicating rapid development into a full storm (Fig. 2). By 0200 UTC on 30 September, the wind speed was back up to 40 kt and the seas had grown to 20 ft.

By 0600 UTC on 30 September, the wind speed was a constant 63–66 kt with gusts to 76 kt. It was now no longer possible to maintain the ship's position. The wind direction started to slowly drive the vessel westward toward the Greenland coast (approximately 48 km distant) and higher concentrations of icebergs. The captain was awakened, called to the bridge, and apprised of the situation. Winds were now gusting to more than 80 kt, and green water routinely coming over the bow threatened the functionality of the forward thruster motors that were necessary to maintain the ship's heading into the wind.

Because of the very short wave periods (8 to 10 s), the ship's stern was now coming out of the water with every wave, causing the propellers to clear the water and overspeed to 200 rpm. The chief engineer set back the power limit to the main shafts to reduce overspeeding of the propellers and reduce the risk of overheating and bearing failure. The result of the reduced power was a loss of position, with the vessel slowly moving south. Even though the ship was buffeted by high winds, we could still maintain a northerly heading. East bias in dynamic-positioning (DP) commands was necessary to prevent the vessel from being blown into ice flows west of site.

With the decision made to give ground to the storm, the vessel's motion then became less violent, but it moved aft at speeds of up to 4 kt. This attitude was made possible only by having the capability of applying lateral force to the forward end of the vessel via the bow thrusters. Lookouts were posted aft to ensure that no icebergs were overtaken.

By midmorning on 30 September, the winds had increased to a sustained 75–78 kt with gusts to 100 kt or greater (100 kt is the maximum indication possible with the shipboard system). This high wind speed (gusts of >70 kt) was sustained for more than 26 hr. As waves broke over the bow, high-velocity sheets of spray raked the vessel. The weather stations were long blown away by this time, but it was estimated that the air temperature was about 3°C (sea temperature). The seas continued to build to 60–70 ft, with recorded pitch angles of up to 14° and rolls to 18°, extraordinary values in DP mode. The BHA remained hanging off on the 500-ton elevators.

At 1245 UTC on 30 September, the port outboard bridge window was blown in by a wave, knocking out both radar displays, denting the bridge wall, and flooding the entire bridge. A group of Sedco and ODP drilling and technical personnel quickly transformed them-

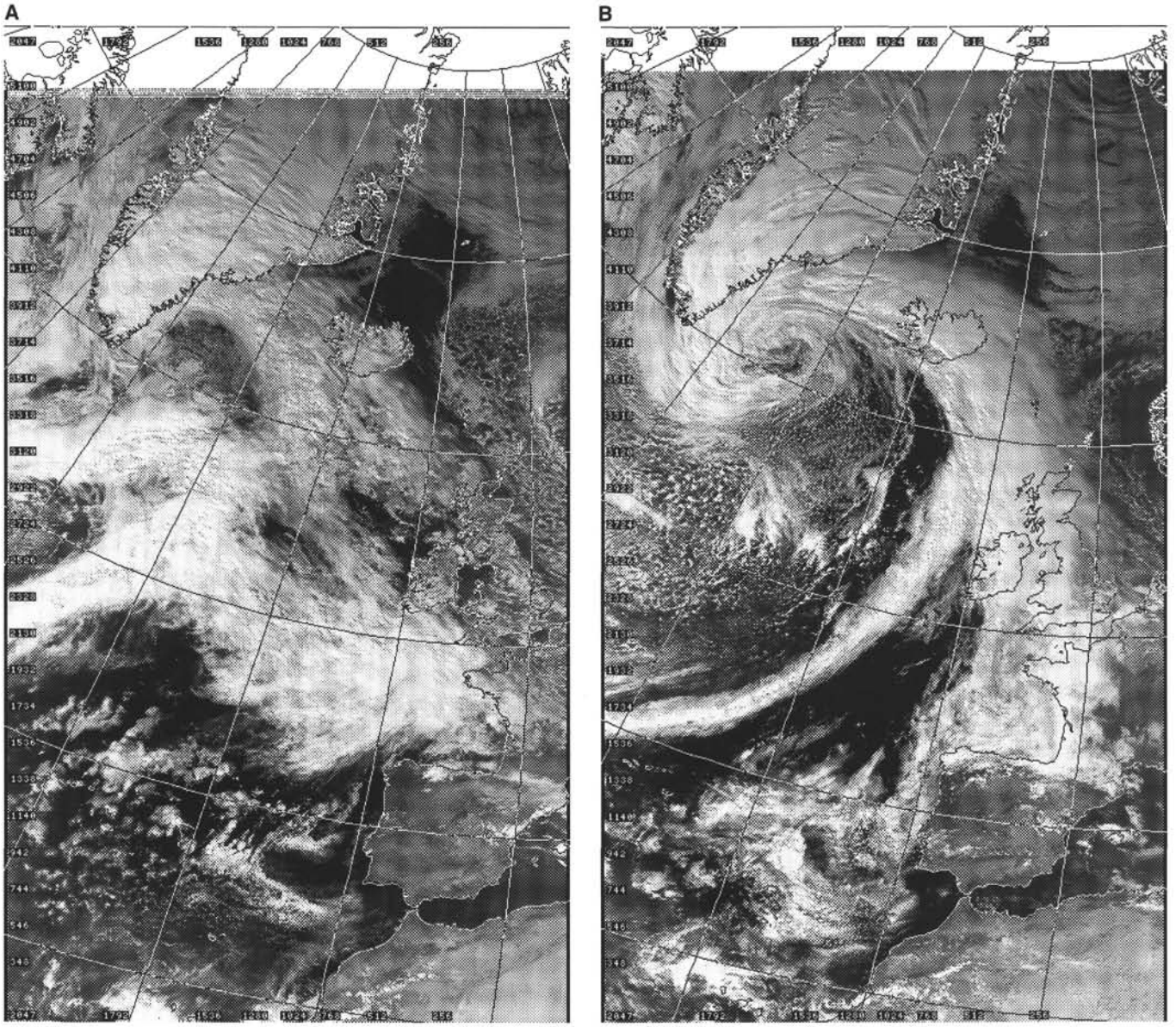

Figure 2. Satellite images of the North Atlantic region at (**A**) 1403 UTC on 28 September 1995 and (**B**) 1408 UTC on 29 September 1995. These images illustrating the rapid buildup of the 29 September storm were taken from the NOAA 12 satellite at an average elevation of 856 km. This exceptional storm developed out of two easterly moving low-pressure systems that merged into a more intense, more northerly moving system than was initially forecast.

selves into a crisis team, built a cover to the open window with plywood, 2″ × 4″ lumber, and tarp, and secured this improvised patch with screws and carriage bolts. During this emergency, many risked their lives by exposing themselves to extremely high winds, very rough seas, and low temperatures as they stood outside the bridge to effect repairs. The efficiency with which the repairs were performed ensured that more water did not enter the bridge.

The large volume of seawater that entered the bridge migrated below decks via electric cable ways. Some forecastle deck compartments were flooded as seawater dripped from around overhead light fixtures. The water came within 1 in. vertically of flooding the DP computer electronics. If the DP computer had been shorted out, the only manner by which heading could have been maintained would have been to steam ahead into the seas with the main propellers. At a minimum, that would have increased the chance of more green water hitting the bridge windows and possibly taking out more glass. The lowest barometer reading of 979.0 mb was made at 1100 UTC on 30 September. After this, the barometer slowly began to rise and the winds slowly, almost imperceptibly, started to decrease.

During the storm, radio contact was lost with *Gadus Atlantica.* A Danish Navy warship in the area and Greenland Command were apprised of the lost communication with the picket boat. At 2100 UTC that day, the vessel reestablished contact with *Gadus Atlantica,* which had been steaming into the storm and was now well north of our location in good shape.

By 0400 UTC on 1 October, the winds had dropped to 57 kt with gusts to 65 kt, but waves remained more than 60 ft in height. At this time, another wave hit the bridge deck and damaged the patched window, spraying the bridge with more seawater and shorting out the sole repaired radar display. The broken patch was quickly repaired.

At 0720 UTC, the forward thruster pod was lost as a result of water entering the motor housing. Several other thrusters were not oper-

ational because of overheating or flooding. Directional control of the vessel was then taken over by the mates on the bridge, supplemented by the remaining thrusters. Luckily, the reduced seas (40–50 ft high) and lowered wind speed made directional control considerably easier, and this method of maintaining heading worked well.

By 1500 UTC, the storm had abated to 37 kt, with seas down to 25 ft. The drill string was then retrieved, and at 1815 UTC the vessel came about with the assistance of the remaining thrusters. After the hydrophones and thrusters were retracted, the vessel began the voyage to Halifax, Nova Scotia, for repairs, signaling an end to drilling operations on Leg 163. The *Gadus Atlantica* accompanied the vessel and provided surveillance of the transit path until one of the radar units was repaired.

LITHOSTRATIGRAPHY

Site 990 was washed to a depth of 182.0 mbsf and rotary cored below that level. Sediments were recovered in Cores 163-990A-1R through 3R (182.0–202.3 mbsf), and the recovered interval is divided into two lithologic units. According to ODP convention, these two units are termed lithologic Unit I and lithologic Unit II, even though data from the nearby Site 915 show that the material above 182 mbsf forms two additional lithologic units. As a result, we correlate lithologic Units I and II at Site 990 with lithologic Unit III at Site 915. Lithologic Unit I is a calcite-cemented mixed-cobble conglomerate, and lithologic Unit II is a clayey volcaniclastic breccia; the ages of both units are unknown, but the ages of the overlying sediment and underlying basalt at Site 915 suggest an early Eocene age for them.

Lithologic Units

Lithologic Unit I

Description: Calcite-cemented mixed-cobble conglomerate
Interval: Sections 163-990A-1R-1 through 3R-1, 76 cm (upper limit may be shallower)
Depth: 182.0–192.36 mbsf (upper limit may be shallower)
Age: Unknown (early Eocene?)

Lithologic Unit I is a calcite-cemented mixed-cobble conglomerate, dominated by clasts of altered basalt, gabbro, and dolerite. These lithologies form 75% or more of the cobbles recovered in Unit I, with quartzite and siliciclastic siltstone forming the remainder of the cobbles. The cobbles are generally rounded to well rounded and range in size from 4 to >12 cm in diameter. The matrix of this conglomerate is poorly represented in the recovered material and is present mostly as thin smears attached to the larger cobbles. Where it was recovered, the matrix is a poorly sorted silty sand, with angular grains, sand-sized mudstone intraclasts, and calcite cement. The similarity of the composition and texture of the large clasts and the matrix to those described for the upper portion of lithologic Unit III at Site 915 suggests that Unit I at Site 990 is the lateral equivalent of Unit III at Site 915.

Lithologic Unit II

Description: Clayey volcaniclastic breccia
Interval: Sections 163-990A-3R-1, 76 cm, through 3R-5, 35 cm
Depth: 192.36–202.3 mbsf
Age: Unknown (early Eocene?)

Lithologic Unit II directly overlies basalt and is dominated by basaltic debris. Clasts in the breccia are predominantly angular and composed of dark yellowish brown (10YR 4/4; see "Lithostratigraphy" section in the "Explanatory Notes" chapter, this volume) altered basaltic material (Fig. 3), although more rounded, slightly altered, light green to light blue basaltic clasts with well-developed alteration rinds are present in Sections 163-990A-3R-2 through 4 (Fig. 4). The

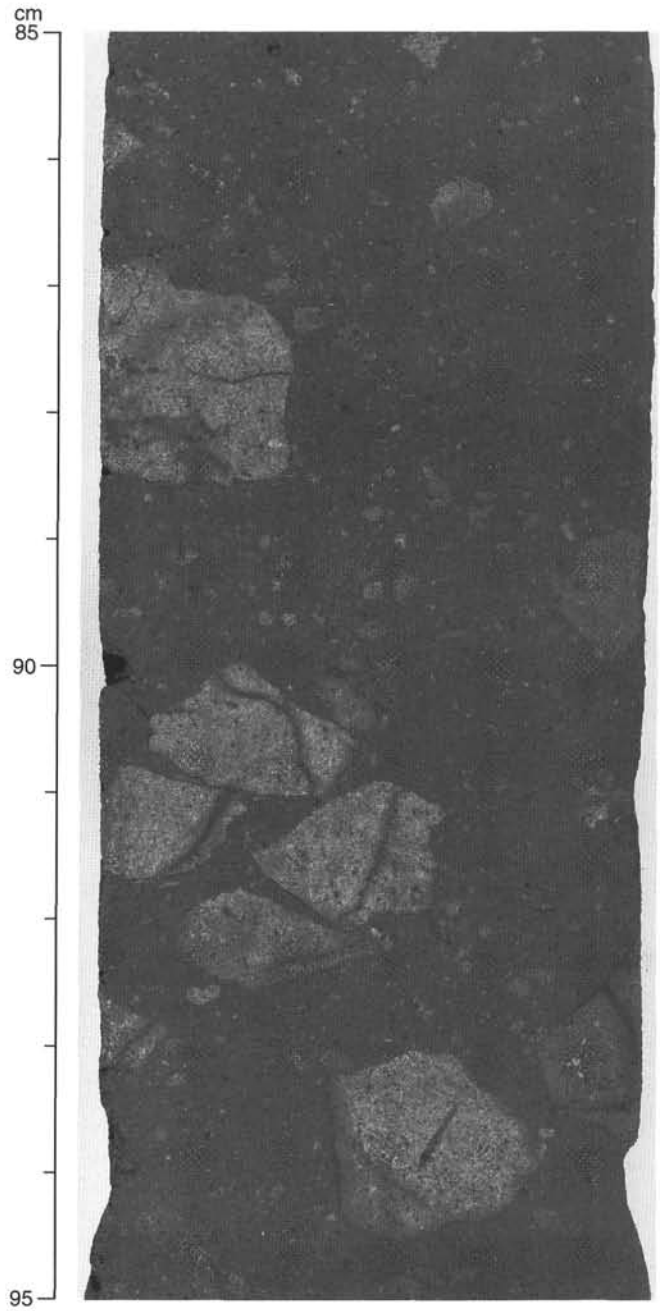

Figure 3. Close-up photograph of Section 163-990A-3R-1, 85–95 cm, showing the angular clasts of altered basalt in lithologic Unit II, the matrix-supported nature of the breccia at this level, and the "fitted fabric" of adjacent clasts.

matrix of the breccia is dominated by clay and iron oxides (derived from the alteration of basaltic material?), with minor well-rounded silt to fine sand-sized quartz grains dispersed throughout. The matrix grades from reddish brown (5YR 4/3) above Section 163-990A-3R-3, 83 cm, to very dusky red (10R 2.5/2) below that level. Above Section 163-990A-3R-3, 70 cm, clast abundances vary enough to produce three intervals with a consistent pattern of variation; in each interval, a basal clast-supported breccia overlying a poorly developed basal contact shows weak indications of stratification and flow and grades upward into a matrix-supported breccia (Fig. 5). Below Sec-

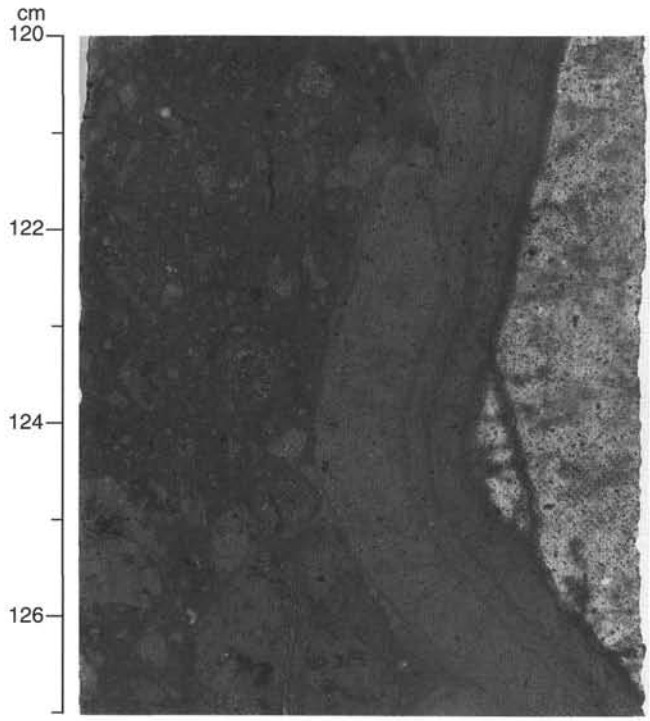

Figure 4. Close-up photograph of Section 163-990A-3R-2, 120–127 cm, showing the edge of a large, rounded basalt clast with an alteration rind approximately 1 cm thick.

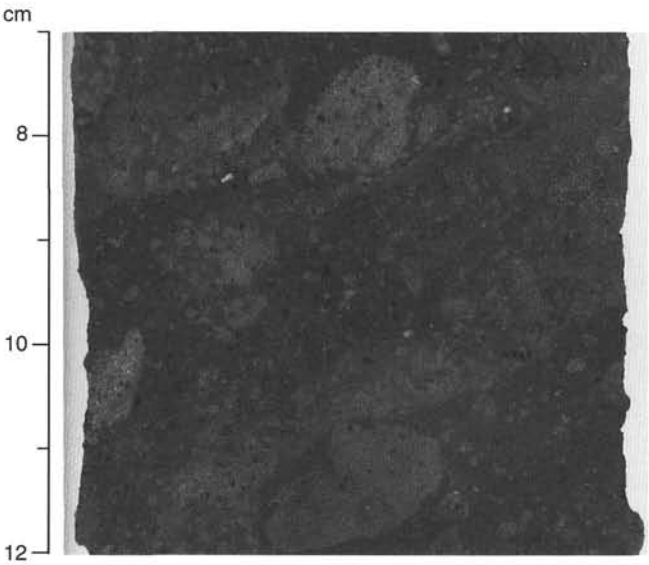

Figure 5. Close-up photograph of Section 163-990A-3R-2, 7–12 cm, showing the clast-rich zone at the base of the uppermost interval indicating flow within lithologic Unit II. Breccia grades upward from clast-rich, poorly developed flow indicators at 11 and 8 cm to matrix-supported breccia.

tion 163-990A-3R-3, 70 cm, the recovered interval is dominated by clast-supported breccia. Within the lower clast-supported breccia, individual clasts become more competent downcore, and clasts in Sections 163-990A-3R-1, 4, and 5 have preserved angular outlines that can be joined between adjacent clasts (Figs. 3, 6). The similarity of the composition and texture of the volcaniclastic breccia to those described for the lower portion of lithologic Unit III at Site 915 suggests

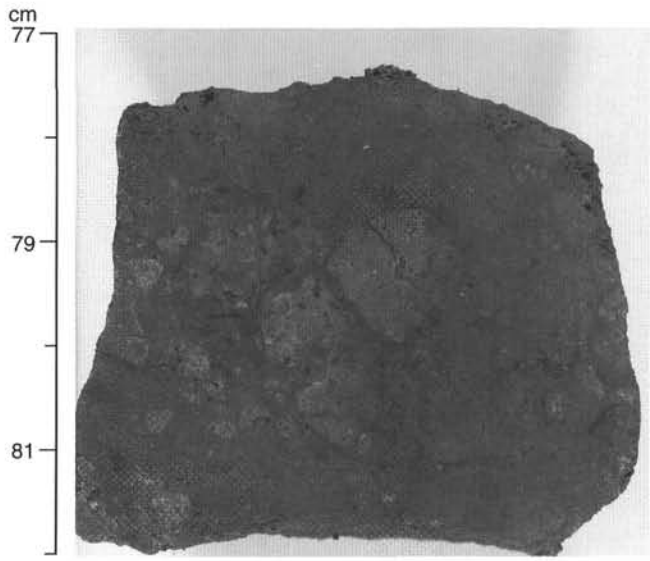

Figure 6. Close-up photograph of Section 163-990A-3R-4, 77–82 cm, showing the angular clasts of altered basalt in lithologic Unit II, the clast-supported nature of the breccia at this level, and the "fitted fabric" of adjacent clasts.

that Unit II at Site 990 is the lateral equivalent of lower Unit III at Site 915.

Additional sedimentary material is present as zones of red, clay-sized to brecciated basaltic material at the tops of flow units within the basalt sequence. This material shows no evidence of transport and redeposition, so it was described as part of the igneous sequence (see "Igneous Petrology" section, this chapter).

Interpretation

The red, clayey to brecciated zones that lie within the basalt sequence are interpreted to be the weathered tops of individual flow units. Similar zones recovered during Leg 152 (Shipboard Scientific Party, 1994) have been described as laterites, indicating deep weathering and the abundant formation of hydrous iron oxides; such soils may also be known as oxisols. Although this preliminary designation will be tested by post-cruise studies, the initial classification of these soils suggests vegetated, warm to temperate, and humid conditions at the time of soil formation.

Lithologic Unit II at Site 990 directly overlies basalt and is dominated by fresh to altered volcaniclastic material supposedly derived from the underlying basalt sequence. The presence of poorly developed flow indicators, the repeated vertical changes between clast-supported and matrix-supported fabric, and the absence of macroscopic pedogenic features (e.g., soil horizons, root traces, and ped structures) suggest that Unit II is not an in situ paleosol. Instead, Unit II appears to be redeposited material, although the predominance of locally derived basalts and weathered basalts, preservation of angular mudstone clasts, and appearance of a "fitted fabric" (Figs. 3, 6) between adjacent clasts suggest that the distance/energy of transport was limited. One possible mechanism for such transport and deposition is by a high-viscosity, matrix-rich sediment gravity flow, such as a debris flow. The characteristics of Unit II suggest that this flow originated from the altered top of a volcanic pile adjacent to Site 990, but it must have also incorporated quartz/quartzite grains from exposed Precambrian source rocks or their reworked derivatives during the relatively short transport history. The same source rocks may have also supplied the coarser grained quartzite clasts in Unit I, and the presence of these source rocks requires some complexity in the outcrop geology of the region at the time Unit II was deposited. The

mechanism that produced such complexity is unknown at present, but it may reflect either (1) fault-produced exposures within or adjacent to the volcanic pile or (2) supply by streams flowing into the area from farther inland.

Lithologic Unit I overlies Unit II and is dominated by larger clasts. The large size of these clasts suggests that they were deposited relatively close to their source areas, and the rounding of these clasts, if not inherited from earlier depositional elements (i.e., reworked clasts), suggests that they were deposited in a high-energy environment, possibly a high-gradient stream or a shallow, wave-influenced marine setting. A third possible environment of deposition—a fan delta—combines high-gradient terrestrial conditions and a high-energy, shallow-marine setting. The high-gradient stream hypothesis requires a reasonable amount of topographic relief, which is consistent with two other aspects of the sedimentary sequence at Site 990. First, debris flows are common in areas with significant topographic relief and rapidly accumulating material, providing an appropriate setting for the deposition of Unit II. Second, faulting could produce both the required topographic relief and the exposures of quartz-bearing source rocks needed to provide the nonigneous components to Units I and II. The primary support for the shallow-marine depositional hypothesis is the position of lithologic Unit I between the underlying subaerially erupted volcanic rocks and the overlying marine sediments. In this scenario, Unit I would be interpreted as a basal transgressive unit; a source for the quartz/quartzite clasts would still be required either within or adjacent to the basaltic pile.

BIOSTRATIGRAPHY

Cores recovered at Hole 990A include a mixed-cobble conglomerate with a silty sand matrix (lithologic Unit I) and a clayey volcaniclastic breccia (lithologic Unit II). Detailed examination of the sediment matrices of these units in thin-section Samples 163-990A-3R-1 (Piece 4D, 90–93 cm) and 163-990A-3R-4 (Piece 4D, 124–127 cm) showed them to be barren of fossils.

PALEOMAGNETISM

Paleomagnetic data were obtained from 20 cores in Hole 990A. Magnetization was not measured for the sediments and dropstones of Cores 163-990A-1R through 4R. Coherent in situ basalt flows, consisting of 13 individual flow units, were recovered in Cores 163-990A-5R through 24R. Igneous Units 1 and 2 have normal polarity and Units 3 through 13 have reversed polarity (Fig. 7).

The paleomagnetic data from the volcanic sequence are based on the analysis of archive-half core sections by the whole-core cryogenic magnetometer. Although the NRM intensities exceeded the measuring range of the cryogenic magnetometer, demagnetization up to 30 mT provided reasonable results by removing between 60% and 95% of the initial magnetization. Discrete samples were measured on the WCC using the cube acquisition mode and on the spinner magnetometer, which functioned for a short time (Table 2 on the CD-ROM in the back pocket of this volume). Magnetic susceptibility measurements made on the whole core using the multisensor track are discussed in the "Physical Properties" section (this chapter). The inclination and intensity measurements from the cryogenic magnetometer are presented in Table 3 on the CD-ROM in the back pocket of this volume together with the susceptibility measurements. Because it was not possible to obtain reliable NRM measurements, the Koenigsberger Q ratios and ratios of NRM to anhysteretic remanent magnetization were not calculated.

The basalts of Unit 1 appear to carry a normal magnetization, which was confirmed by shore-based measurements on discrete samples (Fig. 8A). Measurements on discrete samples of Unit 2, however, are in sharp disagreement with the split-core measurements. The results from the cryogenic magnetometer measurements indicate normal polarity for Unit 2 (with the exception of the altered vesicular flow top), whereas the discrete-sample measurements on the shipboard spinner magnetometer show reversed polarity (Fig. 7). The reversed polarity was encountered in all discrete samples from Unit 2 after removal of the low-coercivity normal magnetization (Fig. 8B) with the exception of the three samples from Cores 10R and 11R (Samples 163-990A-10R-3, 32 cm, 163-990A-10R-4, 101 cm, and 163-990A-11R-2, 5 cm) in which the characteristic magnetization appears to be removed together with the low-coercivity overprint (Fig. 8C). The difference between the shipboard measurements on the cryogenic and spinner magnetometers prompted conducting additional discrete-sample measurements (including thermal demagnetization) on shore immediately after the cruise. Preliminary results of these measurements confirm the polarity obtained from the cryogenic magnetometer (Fig. 7). In consideration of the problems with the shipboard spinner magnetometer, the results of split-core measurements from the cryogenic magnetometer and of onshore measurements of discrete samples are used in the interpretation.

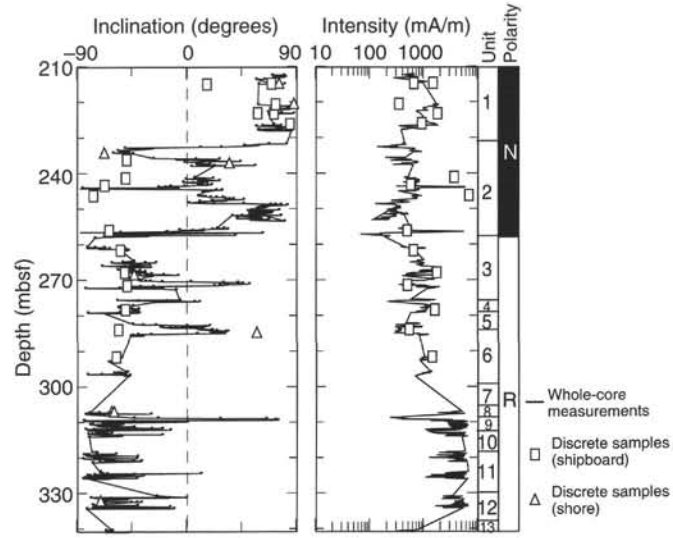

Figure 7. The magnetostratigraphy obtained from Hole 990A showing the inclination and intensity variation in the stratigraphic succession.

Cores 163-990A-12R-2 through 163-990A-24R-3 (Units 3 through 13) have reversed magnetization, confirmed by the discrete-sample measurements made on the cryogenic magnetometer and on shore. Sporadic spikes of normal orientation in this interval are associated with vesicular, highly altered bases and tops of the lava flows, which were possibly remagnetized during hydrothermal alteration. No biostratigraphic data are available for Hole 990A, so the magnetic stratigraphy can be correlated only on the basis of the magnetic anomalies in the area. The normally oriented Units 1 and 2 can be associated with Chron C25n because the results from Leg 152 associated nearby Hole 915 and seaward Holes 914 and 918 with Chron C24r (Larsen, Saunders, Clift, et al., 1994). If this correlation is correct, then the underlying reversely oriented lavas of Units 3 through 13 can be correlated with Chron C25r. The presence of units bearing normal polarity introduces a new complexity to the stratigraphic interpretation of the Southeast Greenland margin basalt sequence, for which resolution must await further shore-based studies, including the confirmation of shipboard paleomagnetic results and $^{40}Ar/^{39}Ar$ dating.

STRUCTURAL GEOLOGY

The basaltic rocks recovered at Site 990 exhibit numerous planar, primary magmatic features that are the most distinctive structural characteristic of the rocks. The most common structures consist of

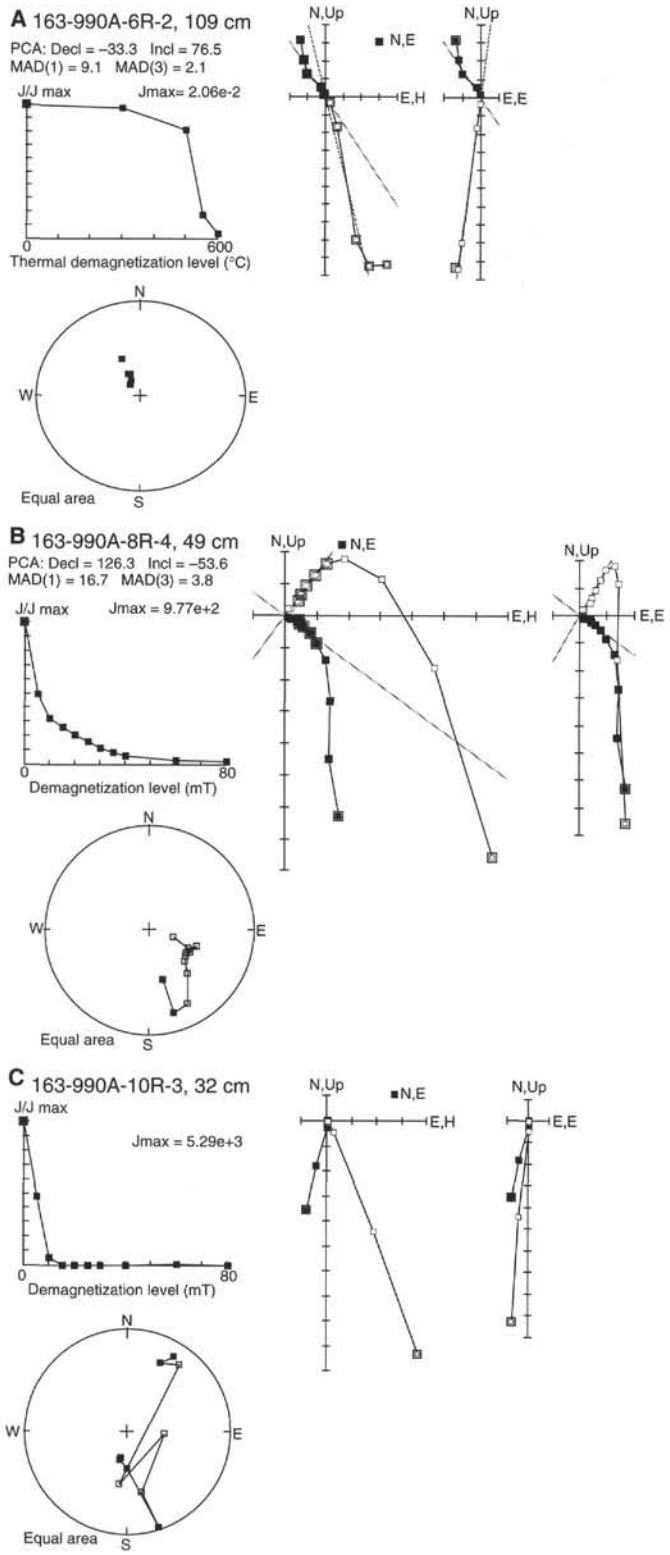

Figure 8. Vector component diagrams (Zijderveld plots) of discrete samples from Hole 990A. The solid symbols represent projections on the horizontal plane, and the open symbols are vector end-points on the vertical plane. **A.** Single-component normal polarity sample from Unit 1. **B.** Sample from Unit 2 carrying a two-component remanence. Demagnetization to 15 mT reveals the reverse high-coercivity magnetization (ChRM). **C.** Sample from the lower part of Unit 2 exhibiting the removal of the low-coercivity primary magnetization together with the drilling-induced overprint.

vesicular layers, elongated patches of filled vesicles, and widely developed diffuse, thin flow bands, which are particularly well developed in Sections 163-990A-9R-1 through 10R-1, 11R-1 through 12R-1, 14R-1 and 14R-2, 15R-1 and 15R-2, 18R-2 through 18R-6, and 19R-3 through 19R-5 (Fig. 9). Many of these magmatic features occur in an almost horizontal attitude (Fig. 10). Although such magmatic features do not necessarily have an originally horizontal orientation, the dominantly low dip suggests that no or only limited tilting or other rotational event has affected the volcanic sequence since its eruption. A few of the magmatic structures in the lower part of the recovered core have very steep dips (Sections 163-990A-12R-1 and 18R-1 through 18R-5). Even in these cases, the steep inclination can be confidently assigned to primary magmatic processes rather than later tectonism and faulting.

The other structures observed in the recovered core reinforce the conclusion of little post-emplacement tectonism, because of the almost undeformed and unfaulted character of the rock. No solid-state plastic deformation is recorded in the core. The only evidence of deformation consists of a relatively dense network of veins and, to a lesser extent, of fractures, some of which show the development of slickensides. Examination of the vein network shows that veins are not homogeneously distributed along the volcanic pile, but are preferentially developed in the upper part of the sequence (Cores 163-990A-5R, 6R, 8R, 10R, 18R, and 19R; Figs. 9, 10). The veins, usually 1–2 mm thick, are commonly lined and filled with green clay. In some veins, two generations of clay have been distinguished. A darker clay lines the outside of the vein and therefore predates the lighter fill in the center. Other minerals less commonly seen in veins include zeolite minerals, carbonates, native copper, and gypsum (see "Igneous Petrology" section, this chapter). The veins do not display any preferred orientation with respect to the core coordinates (see Fig. 10). The tectonic significance of the vein network is not apparent, although some evidence for relative movement is indicated by a few sets of clay-filled veins arranged in an en echelon manner. These vein sets show that the rocks were subjected to incipient flat-lying shearing parallel to the general subhorizontal layering of the volcanic flows (see Sections 163-990A-16R-4 and 18R-4). Section 163-990A-14R-2 shows another set of en echelon fractures that indicate shearing along a vertical plane, although the sense of motion remains undetermined (Fig. 11). The presence of clay filling in these veins indicates that they are not drilling-induced structures.

The few faults observed at Site 990 provide the only examples from Leg 163 of fault-related movement. Slickensided fractures occur in the upper part of the core recovered from the hole (Cores 163-990A-6R, 7R, and 10R). They are generally steeply dipping surfaces, usually coated with clay, and locally arranged as conjugate structures. The direction of displacement is shown by well-developed slickensides that have a range of plunges, but primarily oblique slip with a greater dip-slip component than strike-slip component. The slickensides consist of parallel, very finely spaced, low-amplitude ridges and troughs that commonly form a black, highly polished surface on top of brown clay or gouge. Given the extensional tectonic setting of the region during the Paleogene, as demonstrated by earlier drilling on the Greenland shelf at 63°N (Larsen, Saunders, Clift, et al., 1994), the steep plunges are most likely related to dip-slip normal faulting, whereas the oblique nature of many of the slickensides is due to a lateral component coeval with the extensional structures. The fact that the fractured basalts do not show any evidence of other internal deformation or dislocation in the vicinity of fault surfaces suggests that these are only minor structures recording minor displacements.

The measurements of structural features in the archive half of the core are recorded in Table 4 on the CD-ROM in the back pocket of this volume.

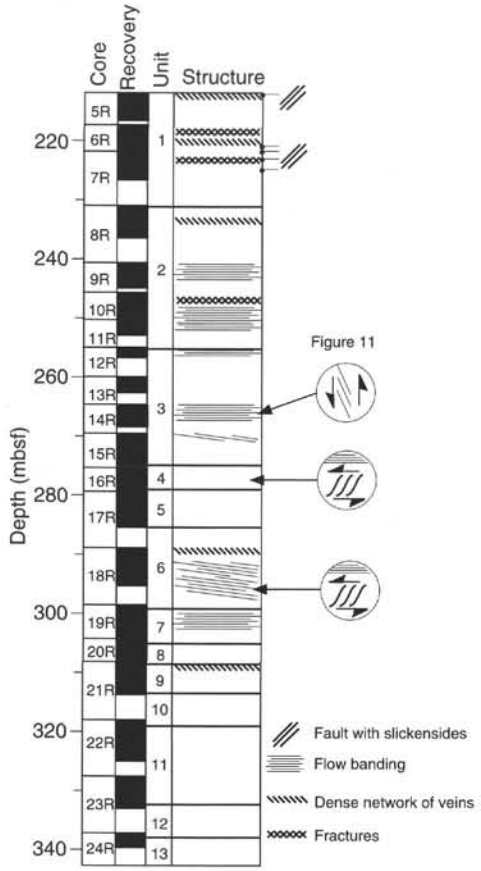

Figure 9. Summary structural log of the drilled section in Hole 990A, showing the distribution of the main planar structures and the location of distinctive individual features.

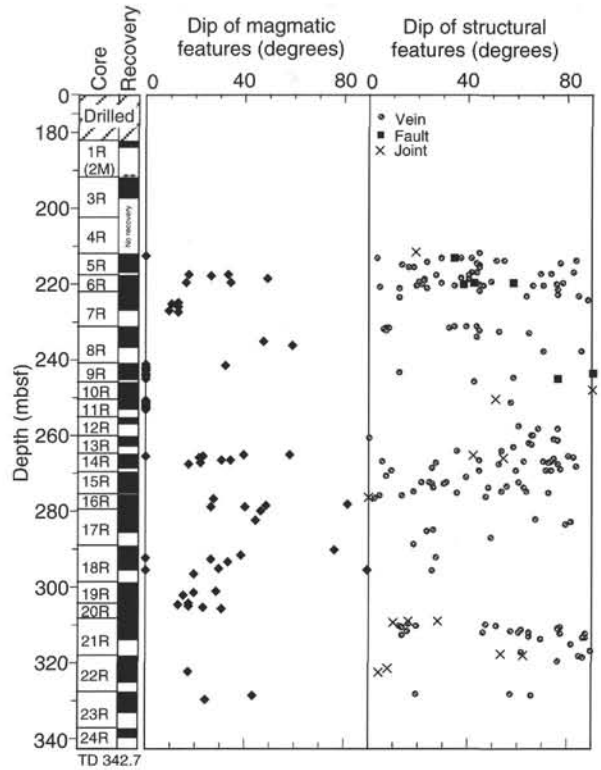

Figure 10. Variation in the dip of flow banding and associated magmatic textural features (left) and amagmatic brittle features (right) measured in core from Site 990.

IGNEOUS PETROLOGY

Lithology

Volcanic rocks at Site 990 are overlain by a coarse conglomerate (lithologic Unit II) consisting of well-rounded cobbles of basalt, diabase, gabbro, and metamorphic rocks in a finer grained matrix. The first igneous unit is in Section 163-990A-5R-1 at 211.9 mbsf. Thirteen igneous units were recognized between this level and the bottom of the hole at 342.7 mbsf. Units were defined to coincide as closely as possible to lava flows, recognized on the basis of changes in phenocryst assemblage or the presence of weathered and/or vesicular flow tops. The location of the tops of the igneous flow units and their curated and calculated thicknesses are given in Table 5. A petrological summary of the volcanic succession is given in Figure 12.

Flow Morphology and Lithology

Lava flows at Site 990 fall into one of three flow types (Fig. 12). The first type ("A") is characterized by a commonly thick (up to 0.5 m), brecciated flow top and a thin (0.2–0.5 m), finely vesicular flow base. The interior is dominated by vesicle-rich segregation pipes and blobs (Fig. 13), in addition to locally prominent banding resulting from local concentrations of mesostasis (Figs. 14, 15). The second flow type ("P") lacks the brecciated top and has a thick upper vesicular zone, massive interior, and pipe vesicles at the base. The third type ("T") is transitional, characterized by a thin breccia and/or vesicular zone at the flow top, some internal banding, and a finely vesicular base. We interpret the thick brecciated flows (type A) as aa flows and the thinner P type as pahoehoe flows. Given the overall thickness and vesicularity of the pahoehoe flows, they were most likely emplaced as proximal sheet flows. Examples of core textures typical of each morphological flow type can be found in the scanned images located on the CD-ROM that accompanies this volume.

The flow units cored at Site 990 range from aphyric to highly olivine or plagioclase-olivine-clinopyroxene phyric basalt. Most units are moderately phyric, with both plagioclase and olivine phenocrysts, although Units 6, 7, and 9 are aphyric olivine basalt (Fig. 12). The olivine content generally decreases upward in the section. Both phenocryst grain size and flow thickness tend to increase upward, with Units 1–3 reaching thicknesses in excess of 15 m (Table 5). Figure 12 also shows that pahoehoe flows (type P) dominate the lower portion of the drilled sequence (Units 8–12) and aa flows compose the upper portion of the sequence (Units 1–3). Transitional-type flow morphologies were found over a stratigraphic interval of ~30 m between Units 3 and 8. Interpretation of T-type flows is aided by *P*-wave velocity and magnetic susceptibility measurements (see "Physical Properties" section, this chapter), which suggest that Unit 6 and possibly Units 4 and 5 are aa whereas Unit 7 appears to be pahoehoe. The upward progression from pahoehoe to aa flow morphologies may reflect an increase in the magma supply rate or migration of the primary vents away from the site.

The top of the volcanic sequence at Sites 990 and 915 (for site location, see "Background and Objectives" section, this chapter) is deeply weathered and oxidized, and all of the lava flow units at Site 990 have oxidized flow tops. Some units are separated by thin (1 cm to at least 5 cm) layers of red soil. Good examples of soil horizons are at the top of Units 3 (Section 163-990A-12R-2 [Pieces 4 and 5, 18–27 cm]) and 7 (Section 163-990A-19R-1 [Piece 7, 54–64 cm]). Similar soil horizons were reported in the Upper Series at Site 917. The presence of soil horizons at both Site 990 and Site 917 shows that

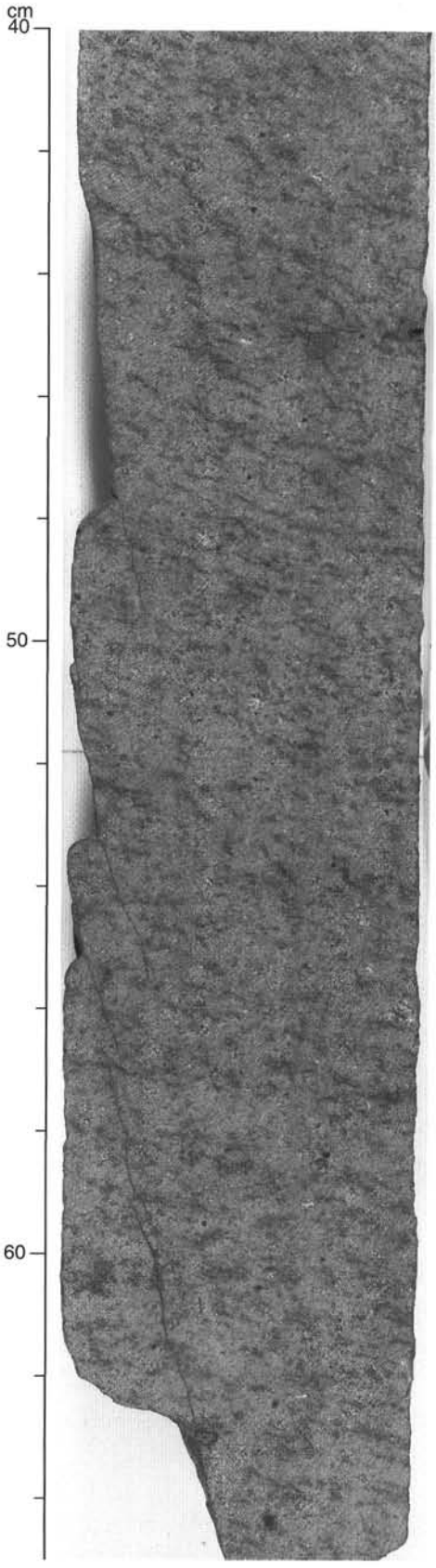

Figure 11. Photograph of Section 163-990A-14R-2 (Piece 5A, 40–65 cm) showing steeply dipping en echelon fractures related to subvertical brittle shearing of the basalts.

Table 5. Location and thicknesses of igneous unit boundaries in Hole 990A.

Unit	Core, section, interval top (cm)	Depth (mbsf)	Curated thickness (m)	Calculated thickness (m)
163-990A-				
1	5R-1, 10	212.0	17.89	19.2
2	8R-1, 15	231.2	22.13	24.8
3A	12R-2, 18	256.0	14.49	17.5
3B	15R-4, 20	273.5	1.72	1.3
4	15R-5, 70	274.8	4.58	4.2
5	16R-4, 62	279.0	5.59	5.7
6	17R-5, 135	284.7	9.87	14.3
7	19R-1, 54	299.0	7.38	6.1
8	20R-1, 100	305.1	4.78	4.3
9	21R-1, 127	309.4	4.53	4.1
10	21R-4, 145	313.5	0.87	5.1
11	22R-1, 82	318.6	10.19	11.6
12	23R-3, 53	330.2	3.88	7.4
13	24R-1, 65	337.6	2.88	—

eruption occurred under subaerial conditions with some time gap between successive flow units.

Primary Mineralogy

The mineralogy and texture of the massive and freshest parts of the 13 igneous units were examined in 15 thin sections. With the exception of Units 6, 7, and 9 (see below) all lavas are moderately to highly phyric with phenocrysts of plagioclase (2% to 15%), olivine (0 to 7%), and augite (trace to 2%) (Fig. 16). Plagioclase, with or without augite, commonly forms intergrown glomerocrysts. Normal and oscillatory zoning and resorption features are common in the anhedral to subhedral plagioclase crystals. Olivine was recognized only as pseudomorphs, and the estimation of modal abundances and textural relations was therefore difficult. In most cases the size of the subhedral pseudomorphs suggests that the olivine crystals formed microphenocrysts. Individual small olivine grains are dispersed and were never found associated with the plagioclase-augite glomerocrysts. Units 6, 7, and 9 differ from the others by carrying only sparse amounts (~1%) of plagioclase and augite phenocrysts and 1%–5% olivine microphenocrysts.

The groundmass of all rocks consists of plagioclase (30% to 50%), augite (20% to 42%), magnetite (1% to 4%), olivine (0 to 4%), and mesostasis (0 to 30%). The groundmass displays intergranular, intersertal, and more rarely seriate and subophitic textures. No significant differences in either primary mineralogy or texture were found between aa- and pahoehoe-type flows.

Major Oxide and Trace-Element Composition

Fifteen samples of lavas collected from the least altered, interior portions of the 13 igneous units were analyzed for major oxide and trace-element concentrations by shipboard X-ray fluorescence (XRF). The composition of two basalt clasts (Sections 163-990A-1R-2, 8–11 cm, and 163-990A-3R-1, 51–56 cm) from the sedimentary unit overlying Unit 1 was analyzed for comparison purposes. These results are reported in Table 6. Additional samples from highly altered flow tops and soil horizons were also selected for XRF analysis. These data are reported in Table 7 and discussed below (see "Alteration" section). Also noteworthy is Sample 163-990A-6R-2 (Piece 2A, 38–40 cm) taken from a vesicle-rich segregation band in Unit 1. The remaining samples are regarded as representative of the bulk composition of individual flow units.

The basaltic clasts recovered from the conglomerate overlying the volcanic sequence at Site 990 include a large (22 cm cored) boulder (Section 163-990A-3R-1, 51–56 cm) resting on the weathered top of the lava succession and a rounded, 5-cm cobble recovered with a rind

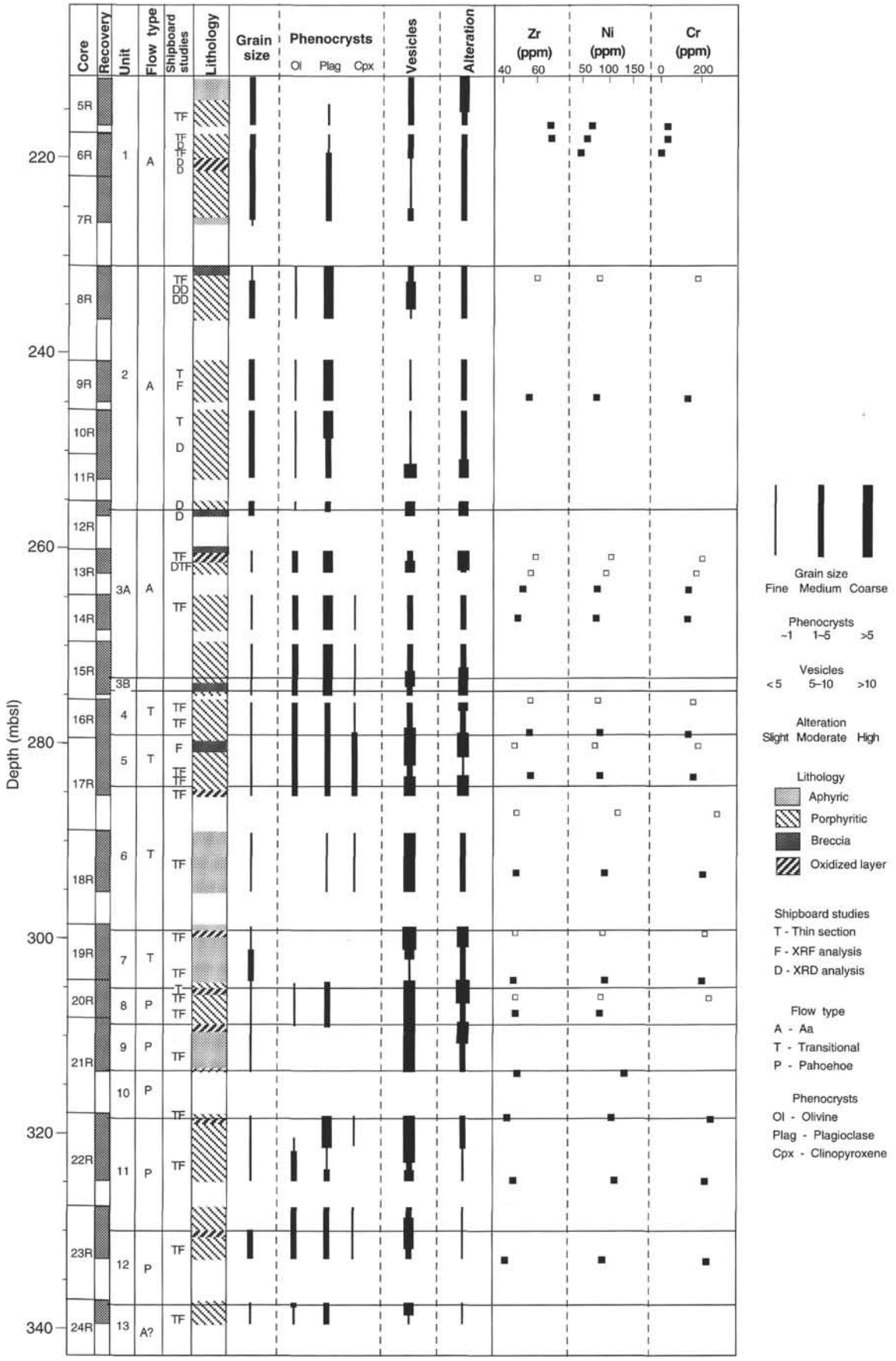

Figure 12. Coring and lithologic summary showing the petrographic and compositional variation of the igneous units at Site 990.

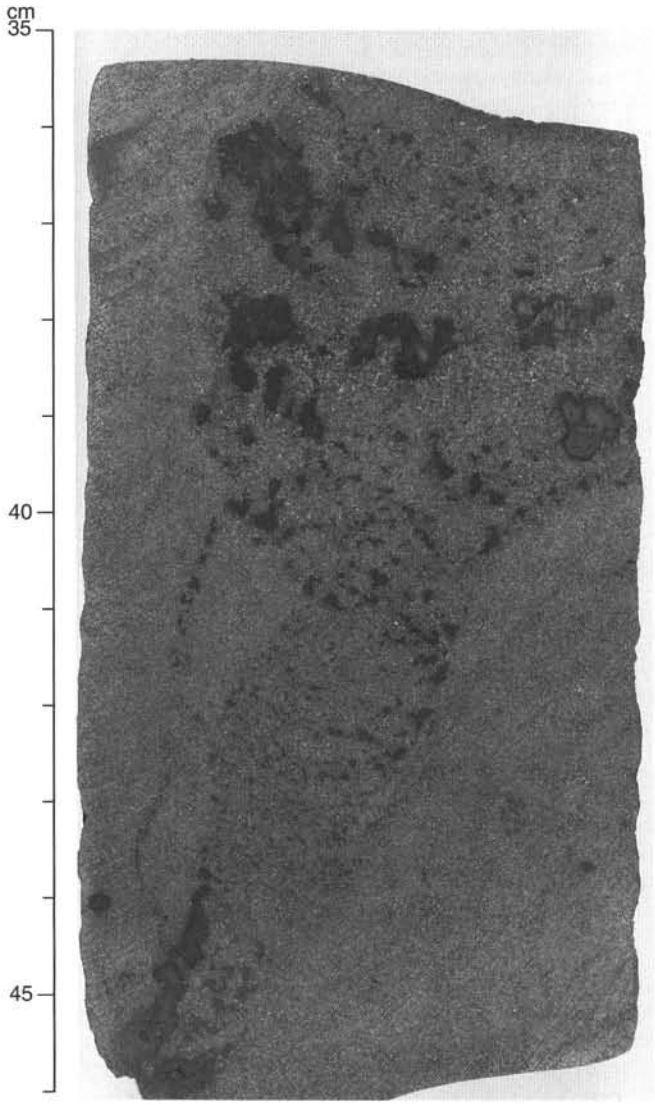

Figure 13. A vesicle segregation pipe/blob from Unit 1, Section 163-990A-6R-1, 35–46 cm. Note the banding of vesicles and groundmass within the upper part of the segregation.

of finer sedimentary matrix still attached (Section 163-990A-1R-2, 8–11 cm). The large clast is compositionally similar to the in situ lava flows at this site, but the smaller clast is quite distinct (Table 6). This smaller clast has high Sr (407 ppm) and Ba (281 ppm) contents similar to lava flows from the Site 917 Lower Series (Larsen, Saunders, Clift, et al., 1994). The striking geochemical resemblance of this clast to Lower Series lavas suggests that rocks equivalent to the Lower Series drilled at Site 917 were exposed to erosion at the time the conglomerate was deposited on top of the Site 990 lava succession. Although further shore-based work is needed to characterize clast affinities with possible source terranes in the region, these preliminary observations indicate relief and erosion of the rifted margin following emplacement of the lavas at Site 990.

In general, the in situ lavas from Site 990 have moderate to high total iron contents, intermediate Mg# (44–65), and low compatible-trace-element abundances (Ni ≤ 132 ppm, Cr ≤ 276 ppm). These lavas are also distinctive in their low abundances of highly incompatible elements (Nb ≤ 3.6 ppm, Zr ≤ 69 ppm, Y ≤ 28 ppm, Rb ≤ 4.1 ppm) and Sr (≤115 ppm).

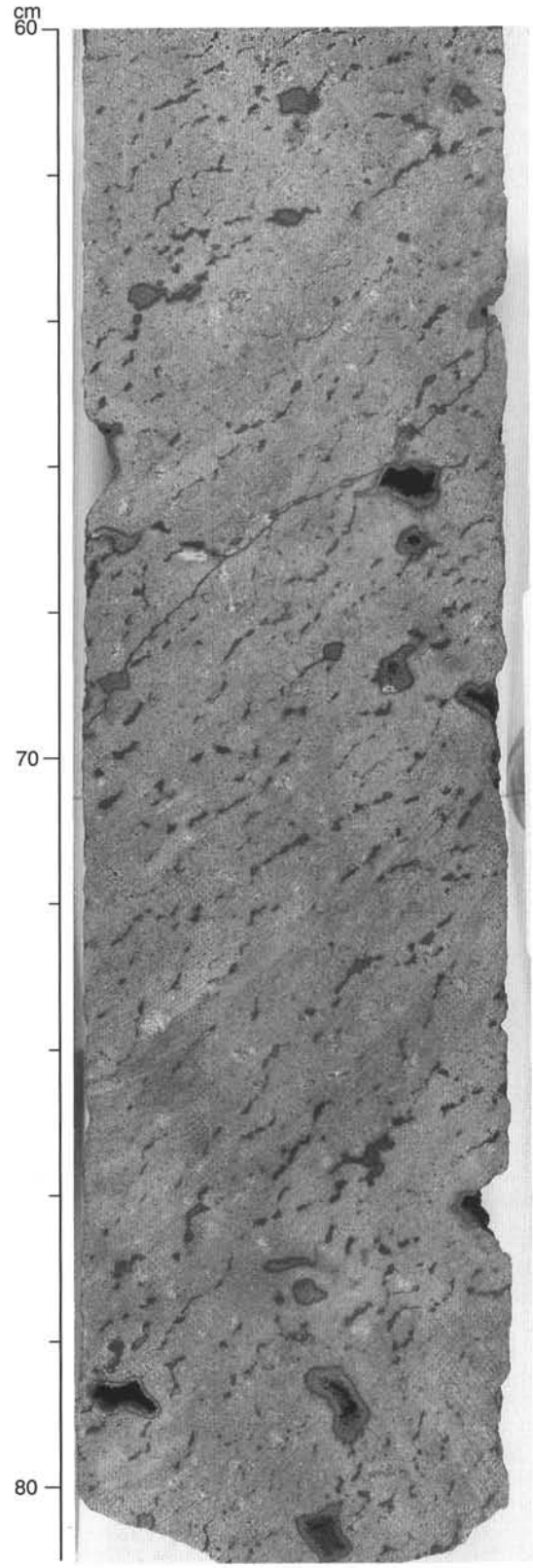

Figure 14. Mesostasis-rich wisps in Unit 4, Section 163-990A-16R-2, 60–81 cm. These concentrations of mesostasis exhibit an approximately constant orientation and commonly contain large, irregularly shaped vesicles.

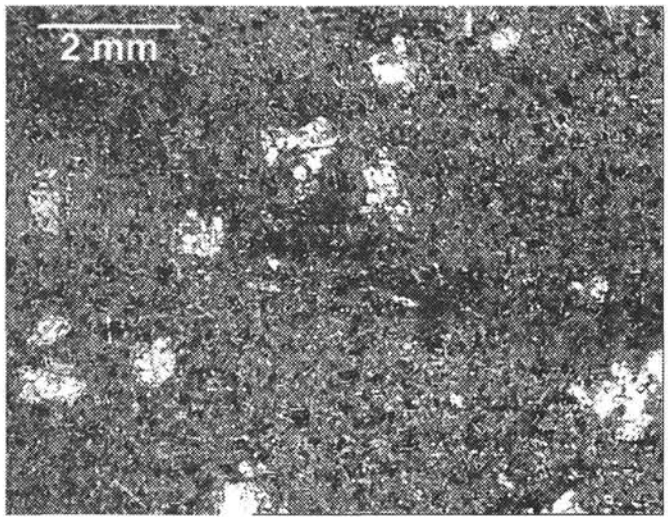

Figure 15. Photomicrograph of an example of the mesostasis-rich wisps that delineate the internal structure of the upper seven igneous flow units at Site 990 (Sample 163-990A-9R-2, 86–90 cm).

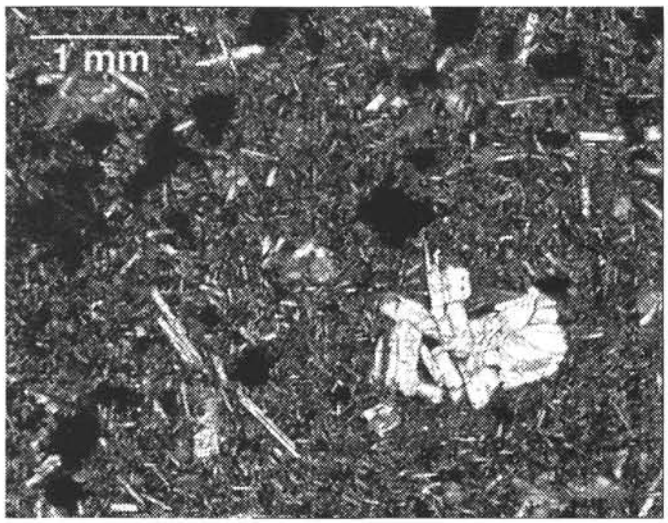

Figure 16. Photomicrograph of a typical highly plagioclase-olivine phyric basalt from Unit 3 (Sample 163-990A-13R-3, 109–110 cm). Note the plagioclase glomerocrysts and dispersed pseudomorphs after olivine (black).

The drilled sequence shows a systematic compositional stratigraphy from base to top. The trends for Zr, Ni, and Cr are shown in Figure 12. Zr increases from ~45 to ~68 ppm from base to top, whereas Ni and Cr decrease from ~110 to ~55 ppm and from ~250 to ~35 ppm, respectively. Nb also increases by over a factor of 2 upward (~1.8 to ~4.0 ppm; Table 6); however, Sr shows no systematic variation.

The vesicle-rich segregation band (Sample 163-990A-6R-2 (Piece 2A, 38–40 cm) collected from Unit 1 is compositionally distinct from its host represented by Samples 163-990A-5R-4, 44–49 cm, and 6R-1, 46–51 cm (Table 6). Compared with the host, the segregation is enriched by a factor of 1.25 to 2 in the incompatible elements Zr, Y, Nb, Ba, and Rb and strongly depleted in Cr (by a factor of 10). The V abundance is also elevated in the segregation compared with the host, which is consistent with the high proportion of modal Fe-Ti oxides present.

Table 6 provides a comparison between the composition of the units recovered at Site 990 and Unit 3 from Site 915. Agreement is very good with respect to all measured elements, suggesting that the lavas cored at Sites 990 and 915 are indeed part of the same succession. On the basis of the well-defined trend shown for Cr at Site 990 (Fig. 12), the Site 915 lava flow (Cr = 145 ppm) corresponds most closely to Unit 3 at Site 990 (Cr = 139–145 ppm). It is more likely, however, that the top of the succession at Site 990 lies below the Site 915 lava flow because the former is located 57 m deeper than the latter.

A primary motivation for drilling at Site 990 was to establish with greater certainty the chemical stratigraphy between the Upper Series recovered at Site 917 and the oceanic succession cored at Site 918 on Leg 152. A comparison of Zr, Sr, and Ni concentrations is shown in Figures 17 and 18. The recovered units from Site 990 (and Site 915) lie well within the compositional fields defined by the oceanic succession (Site 918). Lavas from all three sites (915, 918, 990) are low in both compatible and incompatible trace elements and define coherent trends displaced from the trends shown by the Upper Series at Site 917. We therefore conclude that lavas recovered from Site 990 are part of the oceanic succession, consistent with the conclusion reached by Larsen, Saunders, Clift, et al. (1994) for lavas at Site 915.

The inferred stratigraphic position of the uppermost unit drilled at Site 917 (Larsen, Saunders, Clift, et al., 1994) and the depth of penetration at Site 990 (342.7 mbsf) bracket the transition from the oceanic succession to the Upper Series to less than ~100 m. In view of the striking contrast in the composition of the lavas at Site 990 and the Upper Series at Site 917, this transition probably is abrupt and may represent a hiatus in volcanism or significant change in the magmatic regime. It follows that most of the Upper Series was therefore sampled at Site 917.

Alteration

All rocks recovered from Site 990 are moderately to completely altered by low-temperature secondary phases that replace primary minerals and mesostasis and fill veins and vesicles. The distribution of secondary minerals recorded in the alteration and vein logs for Hole 990A (see the CD-ROM in the back pocket of this volume) is shown in Figure 19.

Most units have highly vesicular and brecciated tops that are strongly recrystallized to clay minerals and iron oxides/oxyhydroxides. The flow tops are vividly colored, and the commonly observed transition from bright red volcaniclastic breccias/sediments through black/maroon clay-rich samples to pink-stained increasingly coherent basalts with strong igneous textures is clearly documented in the color column in Figure 19. Vesicles within the flow tops are large (some are more than 3 cm across), numerous, and generally partially filled by zeolites (Fig. 20) or completely filled by waxy green or brown clay minerals (e.g., Sample 163-990A-12R-2 [Piece 17, 114–118 cm]).

The red, oxidized upper portions and the black/maroon sections of the altered flow tops are strongly recrystallized to clay minerals. Commonly, centimeter-size patches of altered groundmass preserve a relict igneous texture that is visible in thin section, in which clay minerals have pseudomorphically replaced groundmass plagioclase laths. Partially recrystallized groundmass clinopyroxene is generally the only surviving primary phase; titanomagnetite is partly to completely replaced by iron oxides (hematite, maghemite?) or iron oxyhydroxides. Highly brecciated flow tops are commonly cemented by zeolite and calcium carbonate.

The gray flow interiors are moderately altered. Olivine and mesostasis are completely recrystallized to green clay minerals, whereas plagioclase and clinopyroxene are slightly altered to clays and iron oxyhydroxides around the grain boundaries and along fractures and cleavage planes. Alteration of these phases is more intense in the vicinity of fine clay veins. Vesicles are generally lined or partly to completely filled by clay minerals that exhibit a wide variety of colors (green, brown, blue) in different sections downhole. Zeolite-filled vesicles are less abundant in the less altered gray interiors of the flows compared with the highly altered flow tops, and only rare carbonate-bearing cavities were observed (see Fig. 19).

Table 6. Major oxide (wt%) and trace-element (ppm) composition of basalts from Site 990 and Leg 152 Site 915.

Hole:	990A	990A	990A	990A	990A	990A	990A	990A	990A	990A	990A	990A	990A	990A	990A	990A	990A	915A
Core, section:	1R-2	3R-1	5R-4	6R-1	6R-2	9R-3	13R-3	14R-2	16R-3	17R-4	18R-4	19R-4	20R-4	21R-4	22R-1	22R-5	23R-4	24R-2
Interval (cm):	8–11	51–56	44–49	46–51	38–40	87–91	105–109	99–105	105–109	0–5	57–62	102–105	20–25	110–115	33–37	87–92	115–119	60–64
Piece:	2	7	2	2C	2A	3D	10	6B	5	1A	1C	6	1A	5	3	5A	10A	2B
Unit:	Clast	Clast	1	1	1	2	3	3	4	5	6	7	8	9	10	11	12	3
Depth (mbsf):	183.6	192.1	216.5	217.9	219.3	244.4	264.0	267.0	278.8	283.2	293.1	304.1	307.6	313.7	318.2	324.7	332.8	198.7
Major oxides																		
SiO_2	51.1	47.3	50.9	50.6	50.7	50.8	49.8	50.8	51.2	50.4	50.2	50.8	50.6	51.5	50.7	51.5	50.6	50.41
TiO_2	1.30	1.29	1.22	1.21	1.69	0.92	0.93	0.91	0.98	0.95	0.93	0.89	0.88	0.90	0.75	0.87	0.80	0.93
Al_2O_3	20.42	16.48	13.87	13.53	11.50	15.10	14.79	15.01	14.66	14.27	14.30	13.96	15.52	14.62	15.89	14.20	16.11	14.28
Fe_2O_3(t)	8.99	14.75	13.60	13.87	17.88	11.84	12.34	11.81	12.25	12.36	11.32	12.76	12.07	10.58	10.79	11.57	11.32	13.32
MnO	0.08	0.20	0.20	0.21	0.26	0.20	0.21	0.21	0.20	0.25	0.21	0.22	0.21	0.23	0.19	0.24	0.20	0.20
MgO	5.01	8.07	6.27	6.54	6.14	6.88	7.34	7.28	7.17	7.32	8.38	8.00	7.20	8.47	7.42	8.38	6.79	7.53
CaO	8.44	8.45	10.63	10.54	8.41	11.63	11.89	11.89	11.52	12.15	12.07	11.90	11.91	11.56	11.39	11.51	12.20	11.32
Na_2O	3.24	2.32	2.19	2.11	2.20	1.76	1.81	1.72	1.78	1.91	1.71	1.61	1.68	1.74	1.50	1.61	1.72	2.11
K_2O	0.84	0.42	0.40	0.34	0.46	0.36	0.35	0.32	0.34	0.27	0.28	0.37	0.32	0.28	0.32	0.29	0.34	0.22
P_2O_5	0.19	0.09	0.09	0.10	0.14	0.07	0.06	0.06	0.07	0.07	0.07	0.05	0.06	0.06	0.05	0.05	0.05	0.07
Total	99.61	99.37	99.37	99.05	99.38	99.6	99.56	100.01	100.17	99.95	99.47	100.56	100.45	99.94	99.00	100.22	100.13	100.37
LOI	2.00	4.08	1.01	0.78	1.48	1.02	1.69	0.82	1.35	0.93	1.47	0.64	1.90	1.90	2.45	1.76	1.44	1.29
Mg#	56.13	55.67	51.42	51.98	44.08	57.15	57.72	58.59	57.33	57.62	62.95	59.00	57.79	64.76	61.22	62.44	57.93	55.94
Trace elements																		
Nb	3	2	4	4	5	2	3	3	2	2	3	2	2	2	2	2	2	2
Zr	92	63	68	68	86	55	52	49	56	57	48	46	48	49	43	47	42	48
Y	15	20	27	28	35	21	22	21	21	20	19	20	18	19	15	19	16	26
Sr	407	82	96	99	91	115	88	89	106	113	107	73	97	96	88	86	96	76
Rb	5	3	3	2	5	2	2	2	2	2	2	4	2	1	3	1	3	3
Zn	58	87	107	104	116	88	87	85	92	91	84	91	78	83	72	78	78	90
Cu	117	253	227	135	168	104	92	171	101	126	101	79	66	236	65	104	64	107
Ni	86	105	65	55	43	76	78	75	83	83	94	93	83	132	106	112	89	76
Cr	239	146	36	33	4	139	145	139	141	166	217	212	182	276	256	228	235	145
V	314	435	393	366	496	286	316	290	252	312	298	292	259	298	234	228	246	319
Ce	33	25	33	30	43	25	36	25	9	20	24	22	21	14	12	7	15	9
Ba	281	46	67	72	98	99	61	65	23	58	73	44	69	71	61	17	62	28

Notes: ample 152-915A-24R-2 (Piece 2B, 60–64 cm) from Larsen, Saunders, Clift, et al. (1994). Fe_2O_3(t) = total iron as Fe_2O_3; LOI = loss on ignition; Mg# = 100[MgO/(MgO + FeO)] (molecular oxide amounts) with Fe_2O_3/FeO = 0.15. All determinations by X-ray-fluorescence spectrometry (analysts Don Sims and Joel Sparks).

Table 7. Shipboard X-ray-fluorescence analyses of highly altered basalts from Site 990.

Hole:	990A	990A	990A	990A	990A	990A	990A	990A	990A
Core, section:	3R-4	8R-1	13R-1	13R-2	16R-1	17R-1	17R-6	19R-1	20R-2
Interval (cm):	120–124	105–109	80–84	88–92	18–21	73–77	122–126	70–74	39–44
Piece:	25	16B	5C	10A	1B	12	14B	8	1
Unit:	—	2	3A	3A	4	5	6	7	8
Depth (mbsf):	197.2	232.2	260.8	262.4	275.5	280.0	287.0	299.3	305.9
Major oxides (wt%)									
SiO_2	39.4	54.9	53.5	52.0	51.1	59.1	53.8	52.6	51.7
TiO_2	2.00	1.15	1.17	1.10	0.97	0.79	1.08	0.90	0.82
Al_2O_3	26.20	18.27	17.98	16.23	14.73	17.34	14.87	13.42	15.87
Fe_2O_3(t)	27.00	13.87	15.07	14.29	13.26	12.80	14.99	13.18	10.98
MnO	0.28	0.18	0.19	0.22	0.20	0.09	0.15	0.20	0.18
MgO	1.62	5.57	6.43	7.77	6.97	4.48	6.85	7.80	6.60
CaO	0.60	2.76	3.52	6.14	10.11	2.43	4.92	10.17	11.93
Na_2O	0.87	1.55	1.28	1.10	1.53	1.81	1.05	1.46	1.68
K_2O	0.40	0.53	0.40	0.39	0.41	0.97	0.51	0.42	0.33
P_2O_5	0.16	0.01	0.01	0.01	0.06	0.04	0.02	0.04	0.05
Total	98.53	98.79	99.55	99.25	99.34	99.85	98.24	100.19	100.14
LOI	13.87	7.61	9.93	7.78	3.31	10.25	8.75	3.36	2.69
Mg#	12.11	47.97	49.48	55.52	54.68	44.55	51.20	57.60	57.98
Trace elements (ppm)									
Nb	5	2	2	2	2	1	3	2	2
Zr	77	60	60	57	56	47	48	48	48
Y	86	11	21	21	20	9	14	17	18
Sr	33	52	49	41	90	520	43	86	94
Rb	4	5	4	3	4	9	5	4	4
Zn	277	98	100	103	113	65	97	91	65
Cu	73	109	150	171	96	105	119	100	72
Ni	189	81	104	96	79	73	118	90	86
Cr	259	190	210	185	169	195	287	227	248
V	1020	217	278	259	292	101	219	273	253
Ba	ND	16	13	14	47	57	ND	42	55

Notes: Fe_2O_3(t) = total iron as Fe_2O_3; LOI = loss on ignition; Mg# = 100[MgO/(MgO + FeO)] (molecular oxide amounts) with Fe_2O_3/FeO = 0.15. ND = not detected. X-ray-fluorescence spectrometry by analysts Don Sims and Joel Sparks.

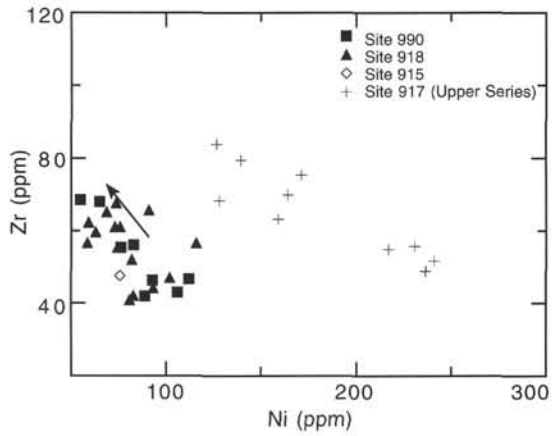

Figure 17. Covariation of Zr and Ni for lavas from Sites 990, 918, and 915 and the Site 917 Upper Series (excluding lavas with >300 ppm Ni). The arrow indicates the direction of upward change in Zr and Ni through the Site 990 sequence. Data for Sites 915, 917, and 918 from Larsen, Saunders, Clift, et al. (1994).

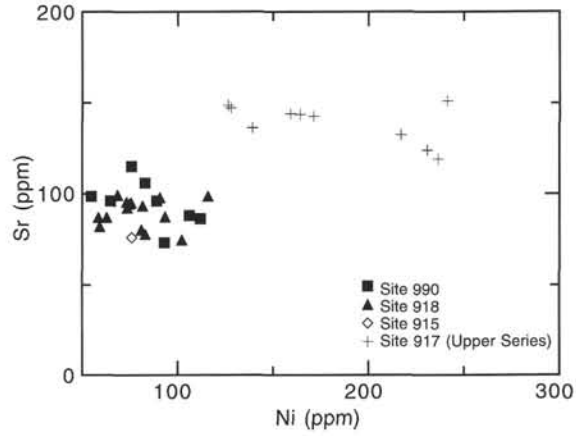

Figure 18. Covariation of Sr and Ni for lavas from Sites 990, 918, and 915 and the Site 917 Upper Series (excluding lavas with >300 ppm Ni). Data for Sites 915, 917, and 918 from Larsen, Saunders, Clift, et al. (1994).

Crosscutting veins are present throughout the drilled section and exhibit a variety of orientations and mineral fillings. Clay minerals are the dominant vein fillings, although zeolite-filled veins are also common. Carbonate veins are less abundant in this hole than in Site 989. Most veins do not have significant halos, although 2–5-cm halos of basalt recrystallized to bright green clay are present in Section 163-990A-5R-2 at the intersections of multiple crosscutting smectite veins.

One occurrence of gypsum was recorded from Section 163-990A-16R-2 (Piece 2, 15–17 cm), where a thick (>20 mm) translucent cleavage slab was recovered within gray lavas from near the top of Unit 4. The presence of this mineral is intriguing, and further geochemical and isotopic studies are warranted.

Small blebs (0.1–2 mm) of native copper are present within the altered mesostasis and occur as a vein and vesicle filling throughout Hole 990A (Fig. 19) in all igneous units except Units 10 and 12. Native copper always occurs with green clay and is absent from regions of visible oxidation (ferric iron staining, iron oxyhydroxides). In Unit 6, a number of green clay + calcium carbonate veins have 15-mm-wide halos with abundant specks of native copper (e.g., Section 163-990A-18R-2 [Piece 1, 58–59 cm]). Halos of disseminated native copper are also associated with carbonate-filled vesicles in Cores 163-990A-18R and 20R. LeHuray (1989) compared the occurrence of native copper in tholeiitic basalts from Site 642 on the Vøring Plateau

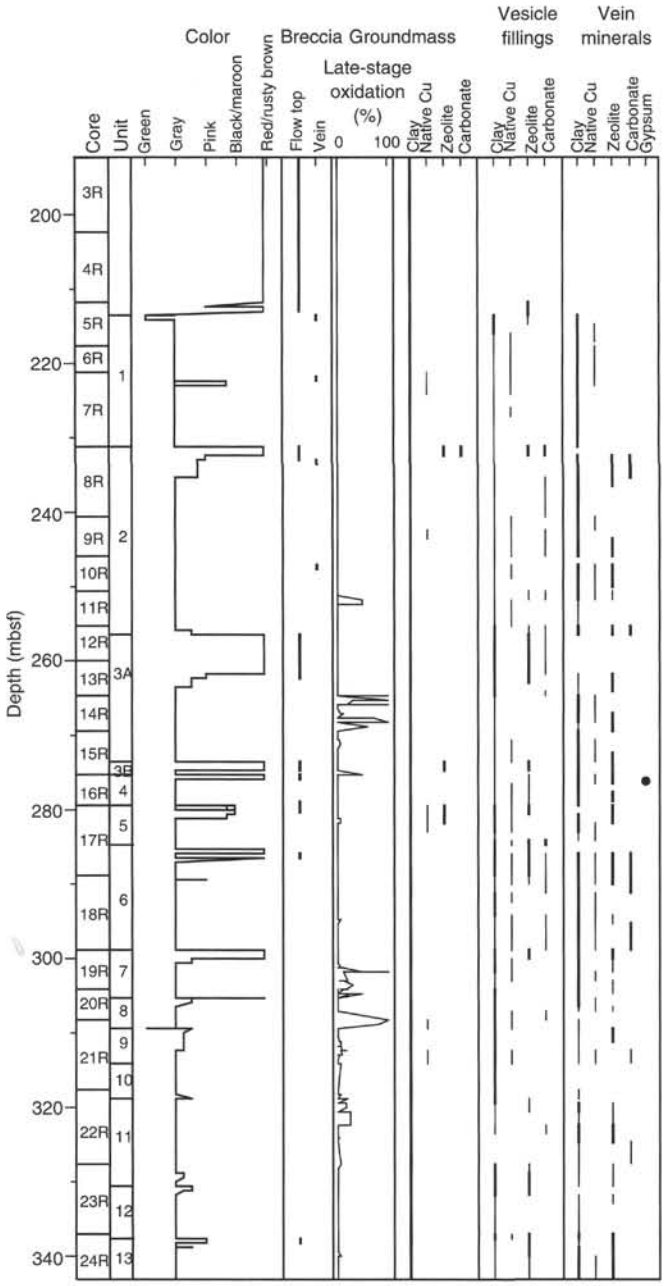

Figure 19. Distribution and abundance of secondary minerals in the groundmass, in veins, and as vesicle fillings, as well as other alteration phenomena in Hole 990A. The macroscopic features and mineral occurrences were recorded as observed in hand specimen from the core. The color is the hue of the bulk rock, with "gray" representing the "background" moderately altered basalts. "Pink," "black/maroon," and "red/rusty brown" record increasing intensity of alteration and recrystallization to highly oxidized assemblages of clay minerals and iron oxides/oxyhydroxides that are generally typical of the clastic volcanic flow tops. "Green" samples are short sections of core where there has been extensive recrystallization of the basalt to green clay minerals (dominantly Mg-smectite) in halos around the intersections of multiple crosscutting smectite veins. The breccia column shows the distribution of clastic volcanic flow tops and breccias associated with highly veined segments of core. Late-stage oxidation provides a measure of the extent of late-stage ferric oxide staining present throughout the core. The distribution of secondary minerals in the groundmass and as vesicles and vein fillings was summarized on a section by section basis. The thin lines record the occurrence of a mineral phase whereas the thick lines denote sections where that particular phase is abundant.

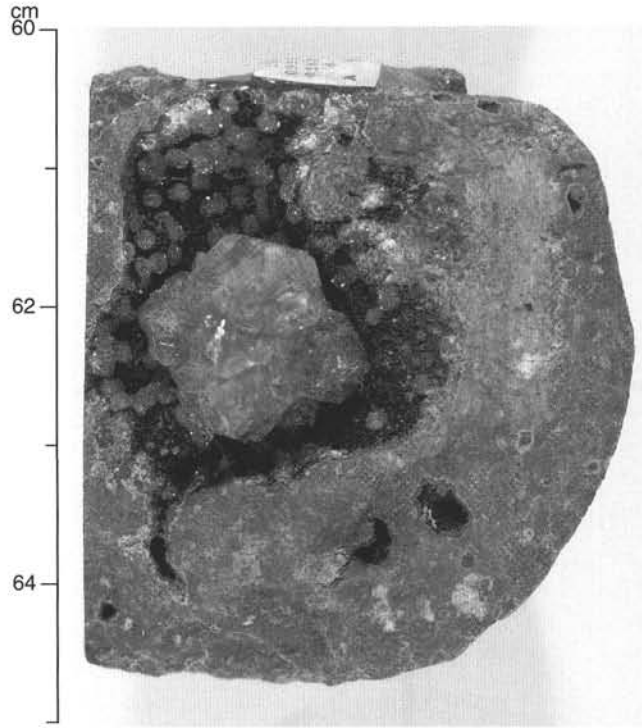

Figure 20. Closeup photograph showing a spectacular, zeolite-filled vesicle from Sample 163-990A-16R-1 (Piece 8, 60–65 cm). The large (≈30 mm), irregular, open cavity is lined with a platy green clay (Mg-smectite). The center of the vesicle is filled with large, partially intergrown, rhombic dodecahedra of yellow chabazite. Smaller, euhedral, white to clear phillipsite exhibiting a more equant habit also lines the cavity.

to the upper Precambrian native Cu deposits of the Keweenaw Peninsula, Michigan, and suggested that similar mineralization processes may have been active. She suggested that the occurrence of native copper relates to initial subaerial weathering followed by seawater-basalt interaction, although this hypothesis has not yet been substantiated with geochemical or isotopic evidence.

Many gray basaltic rocks throughout the core show evidence of late-stage oxidation, commonly exhibited as a faint to strong ferric iron staining that overprints groundmass and vesicle or vein-filling green clay minerals. This staining commonly forms wide halos (>5 cm) around clay-filled fractures or open vesicles. The proportion of late-stage oxidation halos present throughout the core is shown in Figure 19.

Clays, zeolites, carbonate, and gypsum were separated from veins, vesicles, and groundmass from throughout the Hole 990A core and identified by X-ray diffraction (XRD). Descriptions of these samples and their identification are listed in Table 8.

The intense discoloration and extensive recrystallization to secondary minerals of the upper highly vesicular and brecciated portion of the igneous units strongly suggests that these regions were the loci of intense geochemical change. Samples of highly altered flow tops were analyzed by XRF to investigate the relative mobility of both major oxides and trace elements (Table 7). Most trace elements are immobile (Nb, Zr, Sr, Y, V, Zn, Cr, and Ni); however, Rb is strongly enriched in the flow tops and one sample has extremely high Sr, which presumably reflects the presence of secondary calcium carbonate (Fig. 21). Copper is consistently enriched in the altered flow tops (by up to 50%), an observation that contradicts LeHuray's (1989) suggestion that native copper is mobilized from the altered flow tops and redeposited in the interior of flow units by a combination of subaerial weathering and submarine basalt-seawater interaction processes.

Table 8. Minerals from Hole 990A identified by X-ray diffraction.

Core, section, piece, interval (cm)	Description	XRD identification
163-990A-		
3R-2 (Piece 1, 39–40)	Clay	Kaolinite + goethite + hematite
3R-4 (Piece 4, 118–119)	Bright green clay	Trioctahedral smectite
3R-4 (Piece 4, 131–132)	Clay	Trioctahedral smectite
5R-1 (Piece 3, 102–104)	Zeolite	Trioctahedral smectite
6R-2 (Piece 1, 12–12)	Brown clay	Mixed-layer, smectite >> illite
6R-3 (Piece 10, 125–126)	Green clay	Mixed-layer, smectite >> illite (+ magnetite)
6R-4 (Piece 5A, 66–68)	Highly altered basalt	Trioctahedral smectite + magnetite
8R-2 (Piece 11, 65–66)	Carbonate	Aragonite
8R-2 (Piece 17, 108–110)	Carbonate/zeolite	Calcite + phillipsite
8R-2 (Piece 17, 108–110)	Acid-leached zeolite	Phillipsite
8R-2 (Piece 9, 125–125)	Zeolite	Phillipsite
10R-2 (Piece 6, 79–80)	Sheared clay	Mixed-layer smectite > illite
10R-5 (Piece 1, 34–35)	Green clay	Smectite + kaolinite(?) + magnetite
12R-2 (Piece 2, 9–10)	Soapy green clay	Random mixed-layer smectite > illite
12R-2 (Piece 1, 106–107)	Soapy brown clay	Random mixed-layer smectite > illite
13R-2 (Piece 3, 33–34)	Zeolite	Phillipsite
13R-4 (Piece 6, 62–63)	Blue clay (vug filling)	Trioctahedral smectite + minor plagioclase + magnetite
16R-1 (Piece 6, 45–46)	Coarse zeolite (yellow, rhombic dodecahedra)	Chabazite
16R-1 (Piece 15A, 118–119)	Green clay from large vesicle	Dioctahedral smectite(?)
16R-2 (Piece 2, 16–17)	Gypsum (2-cm vein?)	Gypsum
16R-4 (Piece 13B, 96–97)	Vug-filling zeolite (small, white)	Phillipsite
16R-4 (Piece 13B, 96–97)	Coarse zeolite (rhombic dodecahedra)	Clinoptilolite
16R-4 (Piece 15, 130–131)	Zeolite in vein	Clinoptilolite
17R-1 (Piece 13B, 87–88)	Waxy green clay (large vesicle)	Mixed-layer smectite >> illite
18R-1 (Piece 2, 7–8)	Euhedral carbonate filling large vug	Calcite
18R-2 (Piece 1, 105–106)	Green clay from vein	Ordered mixed-layer smectite >> illite
18R-5 (Piece 6, 103–104)	Green clay in vein	Mixed-layer smectite >> illite
19R-1 (Piece 5, 37–38)	Blue clay lining vug ± zeolite	Mixed-layer smectite >> illite
20R-1 (Piece 11, 117–118)	Large rhombic-dodecahedral zeolite (yellow)	Chabazite
20R-1 (Piece 11, 117–118)	Small white zeolite	Clinoptilolite
20R-3 (Piece 2, 45–46)	Flaky green clay from vug	Mixed-layer smectite >> illite
21R-4 (Piece 4A, 44–45)	Euhedral carbonate in vug	Calcite
23R-2 (Piece 7B, 95–99)	Clear zeolite in vesicle	Clinoptilolite
24R-1 (Piece 2, 9–10)	Altered glass	Trioctahedral smectite
24R-1 (Piece 3, 20–21)	Green clay from vein juxtaposed to altered glass	Mixed-layer smectite >> illite + plagioclase

Conclusions

From shipboard petrographic and geochemical studies of the Site 990 lava succession it is clear that the stratigraphic interval between Sites 915 and 917 has not been completely covered. The Site 990 lavas show a small range in chemical composition (Table 6), similar to the Site 915 lava flow and distinct from the Site 917 olivine basalt and picrite flows. The phenocryst assemblages indicate that the magmas were multiply saturated, and the Site 990 lavas vary only in the proportion of olivine, plagioclase, and clinopyroxene. Three observations suggest that the lava-flow sequence at Site 990 may represent a transition from the more basic lavas of the Site 917 Upper Series toward the Site 918 lavas:

1. The proportion of olivine in the phenocryst assemblage decreases upward.
2. The concentrations of MgO, Ni, and Cr decrease and those of incompatible elements (e.g., Zr) increase upward (Figs. 12, 17), suggesting that the erupted magma became slightly more evolved with time.
3. The general increase in flow thickness upward at Site 990 is accompanied by a change in flow morphology from pahoehoe flows at the base to aa flows at the top of the recovered succession. The Upper Series at Site 917 is dominated by thin pahoehoe flows (Larsen, Saunders, Clift, et al., 1994).

Nevertheless, the distinct chemical fractionation trends for the Site 917 Upper Series lavas and lavas from Site 990 indicate that the transition between the successions is most likely quite abrupt and associated with a change in the tectonomagmatic environment.

Importantly, the Site 990 lavas are virtually identical in composition to lavas recovered from Site 918, 72 km farther offshore and in the center of the SDRS (Larsen, Saunders, Clift, et al., 1994). This observation implies that seafloor-spreading-type magmatism was established soon after breakup of the continental margin (represented by the Site 917 Upper Series). The evolved character of the lava flows sampled at Site 990 is consistent with the existence of steady-state magma reservoirs at the time of eruption of the succession. The low concentrations of Nb, Sr, P, Zr, Ti, and Y characterizing the oceanic succession both at Site 990 and Site 918 are indicative of derivation from a depleted mantle source (Fig. 6, "Introduction" chapter, this volume).

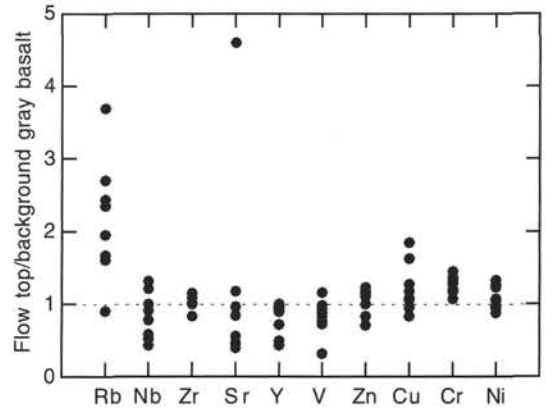

Figure 21. Trace-element concentrations in samples of altered flow tops from Units 2 through 8 in Hole 990A, normalized to concentrations in gray, comparatively fresh basalt from the same flow unit.

PHYSICAL PROPERTIES

Thirteen igneous flow units were recovered from Hole 990A. The high recovery of basalt from the hole enabled a dense sampling for physical properties measurements, including *P*-wave velocity, magnetic susceptibility, bulk density, and thermal conductivity. *P*-wave velocity was measured on both split core sections and discrete sam-

Table 10. *P*-wave velocity and bulk density data measured on seawater-saturated, discrete, 1-in.-diameter minicores from Hole 990A.

Core, section, interval (cm)	Depth (mbsf)	*P*-wave velocity (km/s)	Mass (g)	Volume (cm^3)	Bulk density (g/cm^3)	Comments
163-990A-						
1R-1, 50–54	182.50	4.49	35.03	12.41	2.82	Fine grained (slab, not a minicore)
1R-1, 137–141	183.37	4.20	40.52	14.57	2.78	Fine grained, filled vesicles (slab, not a minicore)
5R-3, 36–38	215.12	4.64	29.46	10.97	2.69	Fine grained, multiple fractures with clayey filling
6R-1, 3–5	217.67	5.77	34.74	11.72	2.97	Fine grained
5R-5, 53–55	217.43	5.70	34.74	11.72	2.97	Fine grained
6R-2, 23–25	219.13	5.65	34.84	11.78	2.96	Fine grained, extensive subvertical fracture with native copper
6R-3, 135–137	221.75	5.44	34.71	11.87	2.92	Fine grained
7R-1, 119–121	222.59	5.48	31.55	10.78	2.93	Fine grained with large vugs partially filled with clay or zeolite
7R-5, 7–9	227.28	5.87	34.01	11.38	2.99	Fine grained, subhorizontal fracture
8R-2, 117–119	233.70	5.84	30.40	11.28	2.70	Coarse-grained basalt with altered feldspar + green clay
8R-4, 4–6	235.46	5.17	33.28	11.59	2.87	Coarse-grained, altered feldspar + green clay, near alteration front
9R-1, 29–31	240.99	5.89	29.77	10.00	2.98	Fine grained with small, isolated, clay- or zeolite-filled vesicles + subhorizontal lineations
9R-3, 111–113	244.68	5.80	34.57	11.70	2.95	Fine grained with small, isolated, clay- or zeolite-filled vesicles + subhorizontal lineations
10R-1, 12–14	245.82	5.94	32.40	10.85	2.99	Fine grained with small, isolated, clay- or zeolite-filled vesicles + subhorizontal lineations
10R-4, 101–103	251.07	6.10	33.17	11.15	2.97	More altered, clayey zone
11R-1, 79–81	251.09	6.24	39.15	13.16	2.98	Fine grained with small, isolated, clay- or zeolite-filled vesicles + subhorizontal lineations
12R-1, 3–5	255.03	6.24	35.38	11.84	2.99	Fine grained with small, isolated, clay- or zeolite-filled vesicles + subhorizontal lineations
12R-1, 125–127	256.25	5.39	34.20	12.13	2.82	Altered, with semiparallel + subhorizontal + elongated vesicles
13R-2, 141–143	262.89	5.14	30.96	11.08	2.80	Pinkish altered basalt
13R-4, 36–38	264.61	5.69	31.89	10.90	2.93	Large vugs filled with green clay
14R-2, 94–96	266.92	5.75	32.53	11.17	2.91	Prominent subhorizontal bands
14R-4, 4–6	268.38	5.31	28.88	10.11	2.86	Clayey areas, wide banding
15R-1, 89–91	270.49	5.93	37.84	12.79	2.96	Dark, inclined, and parallel banding
15R-2, 101–103	271.82	5.98	34.49	11.53	2.99	Nearly vertical fracture, filled with clay
15R-3, 128–130	273.59	5.16	33.52	12.00	2.79	Highly altered, purplish basalt
15R-4, 67–69	274.35	2.80	59.89	25.87	2.32	Highly altered, reddish basalt (slab, not a minicore)
16R-1, 4–6	275.34	5.02	30.86	11.51	2.68	Reddish altered basalt with many round vesicles
16R-2, 41–43	277.12	4.76	31.30	11.16	2.81	Angled, elongate, parallel, clay-filled vesicles
16R-4, 110–112	280.21	4.47	30.03	11.35	2.65	Highly vesicular, rounded, zeolite(?) filled
17R-2, 78–80	281.54	5.06	31.92	11.75	2.72	Highly vesicular, large, rounded, zeolite(?) filled
17R-4, 62–64	283.77	5.49	33.33	11.44	2.91	Fine grained
17R-5, 111–113	285.37	3.08	25.19	10.77	2.34	Highly altered, muddy vesicles, vertical fracture
18R-1, 77–79	289.67	4.80	27.71	10.14	2.73	Segregation bubble or pipe present
18R-4, 126–128	293.83	5.55	37.13	12.80	2.90	Fine grained with clay-filled, irregular vesicles
18R-6, 69–71	296.03	5.85	35.07	11.86	2.96	Fine grained with horizontal, elongate, clay-filled vesicles
19R-1, 39–41	298.99	5.21	32.08	11.51	2.79	Pinkish with many small vesicles and a large, clay-lined vesicle
19R-1, 112–114	299.72	4.77	26.67	11.93	2.24	Pinkish with many large, irregular vesicles filled with clay + zeolite
19R-2, 27–29	300.37	5.44	28.36	10.35	2.74	Pinkish with many vesicles and segregation bubbles
20R-1, 30–32	304.50	5.01	35.40	12.91	2.74	Fine grained, segregation bubbles, clay-filled vesicles
20R-2, 3–5	305.54	4.58	26.57	10.03	2.65	Pinkish, altered basalt with irregular vesicles filled with clay
21R-1, 8–10	308.28	5.43	31.79	11.32	2.81	Coarse grained with clay-filled vesicles
20R-4, 102–104	308.37	5.07	33.08	12.01	2.75	Coarse grained with clay-filled vesicles
21R-3, 56–58	311.67	4.92	27.61	10.21	2.70	Pinkish, altered basalt with irregularly shaped vesicles
21R-4, 104–106	313.65	4.97	31.06	11.03	2.82	Medium to coarse grained with small, irregular, clay-filled vesicles
22R-1, 98–100	318.88	3.90	26.41	11.16	2.37	Altered basalt with irregularly shaped vesicles, some lined with clay
22R-2, 94–96	320.30	5.02	31.73	11.46	2.77	Fine grained with small, rounded, clay-lined vesicles
22R-4, 52–54	322.80	5.66	26.18	8.92	2.93	Medium to coarse grained
23R-1, 13–15	327.63	5.36	32.09	11.37	2.82	Medium to coarse grained with horizontal, dark lineations
23R-1, 119–121	328.69	5.00	29.73	11.20	2.65	Pinkish altered basalt with irregular vesicles lined with white + green clay
23R-3, 84–86	331.06	4.44	26.13	10.08	2.59	Altered with vesicles filled with clay + zeolite ± calcite
23R-4, 59–61	332.23	5.44	29.87	10.83	2.76	Some altered, clayey areas with minor vesicles
Mean		5.21			2.80	
Standard deviation		0.71			0.18	

Notes: Salinity = 0.032; pore-fluid density = 1.022 g/cm^3. The comments reflect changes in rock and/or sample characteristics. Velocity measurement error is ±0.03 km/s.

ples (minicores) using the Hamilton Frame velocimeter. Bulk density was measured on both whole core sections and minicores, whereas magnetic susceptibility was measured directly on whole core sections only. Thermal conductivity measurements were performed on selected pieces using the half-space line source method described in the "Physical Properties" section of the "Explanatory Notes" chapter (this volume).

Acoustic Velocity

P-wave velocity was measured on seawater-saturated split core sections using the Hamilton Frame velocimeter in the same manner as described in the "Site 989" chapter "Physical Properties" section (this volume). The split-core velocity measurement technique permitted compilation of an extensive set of *P*-wave velocity values (978 total) from Hole 990A. A carefully selected set of minicore samples (51 total) from throughout the recovered core was also measured under seawater-saturated conditions using the Hamilton Frame velocimeter. The velocity data for the split cores are listed in Table 9 (on the CD-ROM in the back pocket), and for the minicores in Table 10 (in text and on the CD-ROM). The velocity data are also plotted in Figure 22, along with the minicore density measurement values.

At first glance, the split-core velocities appear to vary wildly, but, when compared with textural variations (see "Igneous Petrology" section, this chapter), a direct correlation can be found between *P*-wave velocity and petrologic data. For instance, velocities are ~2–3 km/s near the flow tops of units interpreted to be aa or transitional in origin and increase to about 5.5 km/s near the central, more massive sections of all igneous units. Toward the bases of the flows, the velocities again decrease to the values present near the flow tops, specifically, ~2–3 km/s. This velocity variation appears to be directly related to changes in porosity within each igneous unit. The same type of correlation between *P*-wave velocity (or modulus) and porosity was mentioned in the "Physical Properties" section of the "Site 989" chapter (this volume).

P-wave velocities measured on minicores show velocity values similar to those of their split-core counterparts (see Fig. 22), and both sets of measurements can be compared to velocities derived from large-scale seismic profiles and downhole logs. Downhole logs in Hole 917A (located ~3 km landward of Hole 990A) and seismic re-

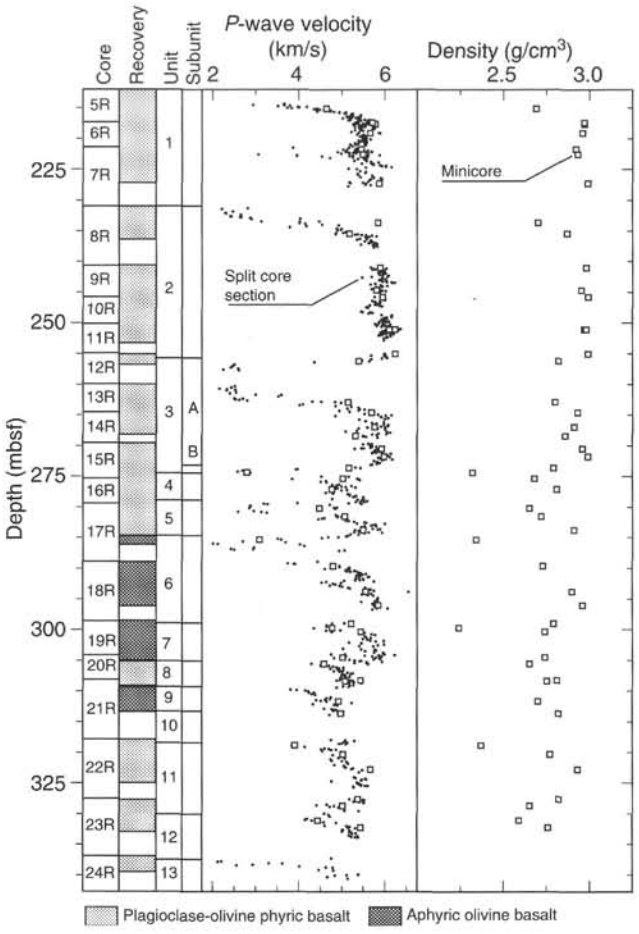

Figure 22. Downcore profile of *P*-wave velocity and density measurements from the igneous units of Hole 990A. Note the low velocity values near flow tops, especially in the thick Units 1, 2, and 3.

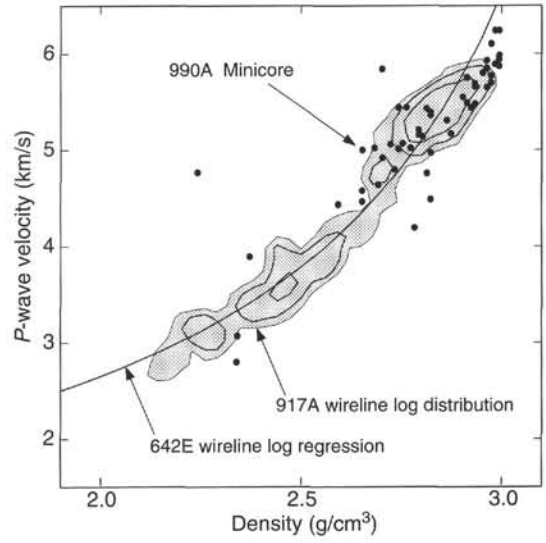

Figure 23. *P*-wave velocity vs. density plot of Hole 990A minicore measurements. Note the nonlinear velocity-density relationship based on wireline log data in Holes 917A and 642E (Planke and Cambray, in press; Planke, 1994). The Hole 990A minicores sample primarily high-velocity, high-density intervals.

flection stacking velocities show average *P*-wave velocities of about 4.1 km/s (Planke and Cambray, in press), whereas the mean split-core *P*-wave velocity measurement from Hole 990A is 5.15 ± 0.77 km/s. This difference of about 1 km/s represents the bias in the better recovery of basalts from within the more massive, central, higher *P*-wave velocity regions of the flow units. A plot of minicore *P*-wave velocity and density measurements from Hole 990A is shown in Figure 23. Also shown is a regression curve from the wireline logs run in Hole 642E (Vøring Plateau) and frequency distribution of velocity and density data points obtained from wireline logs from Hole 917A. It can clearly be seen from the figure that the minicore measurement values are also biased toward the higher velocity and density domain and are not distributed in a fashion at all similar to the log data from Hole 917A.

Index Properties

Bulk density was measured on whole cores at 2-cm intervals using the GRAPE on the MST. The density values, counting rates, and core diameters are listed in Table 11 on the CD-ROM in the back pocket of this volume. The downcore log of GRAPE density, along with the flow units, is shown in Figure 24. The low bulk density measurement values (e.g., <1.8 g/cm^3) are caused by gaps (air) between individual core pieces. Moderately low bulk density values (e.g., 1.8 to ~2.4 g/cm^3) may be due to alteration zones, as well as smaller core diameters. The average bulk density derived from the GRAPE measurements is 2.6 g/cm^3. In contrast, the average bulk density measured on the minicores is 2.8 g/cm^3. This large difference of 0.2 g/cm^3 is probably due to the spatial resolution of the MST measurements. Average values of MST-type data may need a systematic correction. Thus, individual MST measurements performed at known locations on known pieces together with a comparison with minicore measurements may be the preferable method of data analysis.

In general, the density data show similarities to the split-core velocity data. Specifically, values at the top and base of each unit are low, whereas, high values are present in the central part. This characteristic behavior can be seen clearly from the data for igneous Unit 3 in Figure 25. These observations have also been described for the log data from Hole 642E (e.g., Eldholm, Thiede, Taylor, et al., 1987; Barton et al., 1989; Delius et al., in press; Planke, 1994) and Hole 917A (Planke and Cambray, in press).

Magnetic Susceptibility

Magnetic susceptibility was measured at a sampling interval of 2 cm on all whole cores recovered from Hole 990A. The depth variation in measurement values for the flow units is shown in Figure 26. The data values are tabulated in Table 12 on the CD-ROM in the back pocket of this volume. These values range from 100×10^{-5} SI to greater than 5000×10^{-5} SI, with a majority of the values at about 1000×10^{-5} SI. The highest magnetic susceptibility values approach 5000×10^{-5} SI and are present near the top of Unit 2 and within Units 3, 5, and 6. The very low susceptibility values are due not only to lower magnetic carrier contents, but also to gaps between individual pieces within the core sections.

The magnetic susceptibility data reveal inconsistent behavior within each unit. However, when the entire cored interval is considered, an overall trend toward lower values with depth is revealed. This trend correlates with a reduction in grain size with depth within Hole 990A (see "Igneous Petrology" section, this chapter). This same correlation can be seen from the data gathered at Hole 989B; namely, smaller grain size correlates with lower magnetic susceptibility values (see "Physical Properties" and "Igneous Petrology" sections, "Site 989" chapter, this volume). In addition, a reduction in the variability of the magnetic susceptibility values is consistent with a shift from aa to pahoehoe flow morphologies (compare with Fig. 12). The exact reason(s) for this correlation is not readily apparent. High susceptibility values are typically found in thick aa flows (i.e., Units 1, 2, and 3; see Fig. 26). The amount and size of the magnetic particles

Table 13. Thermal conductivity measured with the half-space line source technique on polished, split core sections.

Core, section	Depth (mbsf)	Thermal conductivity ($Wm^{-1}K^{-1}$)					Average	Standard deviation
163-990A-								
6R-2	256.90	2.14	1.84	1.77			1.92	0.20
9R-3	244.83	1.80	1.92	2.05	2.00		1.94	0.11
14R-3	266.28	1.93	2.43	1.86	2.25	2.00	2.10	0.24
19R-3	302.76	1.74	2.20	1.80	1.89	1.72	1.87	0.20

Note: Needle 326.

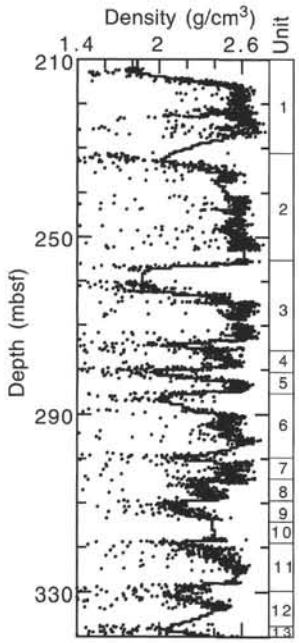

Figure 24. Whole-core GRAPE density vs. depth plot for Hole 990A. There is a large variation in density within the individual igneous units. The lowest densities appear near the unit tops, which is especially apparent in the thicker Units 1, 2, 3, and 6. The points reflect raw data; the line represents a 15-point running average.

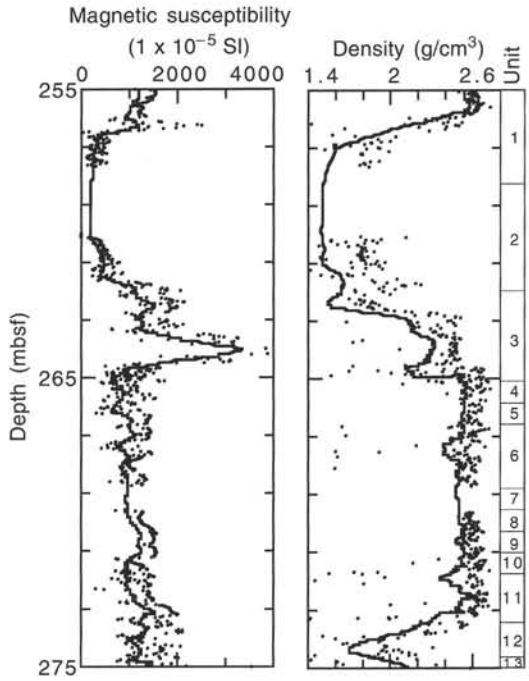

Figure 25. Magnetic susceptibility and bulk density vs. depth for igneous Unit 3 from Hole 990A. The variation in bulk density displays a characteristic behavior for the thicker flows from this hole, with lower density values measured near the flow tops and high density values near the central, more massive regions. Susceptibility variation within a single igneous unit does not show the same trend. The dots represent raw data, and the line through the data points represents a 15-point running average.

are possibly related to variable cooling histories within flows, thus affecting the susceptibility values.

Thermal Conductivity

Three core pieces from Hole 990A were chosen for thermal conductivity measurements. The half-space line source method (as described in the "Physical Properties" section, "Explanatory Notes" chapter, this volume) was used for the measurements, and the data are tabulated in Table 13. The measurements were performed in a water bath under slight overburden pressure on polished split-core pieces. The average thermal conductivity values near 2 $Wm^{-1}K^{-1}$ for samples from Hole 990A agree well with those for samples measured from Hole 989B (see "Physical Properties" section, "Site 989" chapter, this volume).

Summary

The physical properties measurements (*P*-wave velocity, bulk density, and magnetic susceptibility) obtained at Site 990 show striking variations within the 13 igneous units. In general, *P*-wave velocity and bulk density values are low (2–4 km/s and 2.3–2.6 g/cm^3, respectively) near the flow tops and bases and are much greater (~6 km/s and ~3.0 g/cm^3, respectively) near the massive unit interiors. This contrast is most likely the result of variation in the aspect ratios and asperity heights of the void spaces. Void space variations have been shown to have large effects on the acoustic properties of rocks (e.g., Birch, 1961; Cheng and Toksöz, 1979; Carlson and Gangi, 1985). Interflow variations in void space morphology are described on the visual core description forms in the section following the site chapters (this volume). The magnetic susceptibility values are generally higher near the flow tops than at the centers or bases of the flows. These high values are associated with an increase in alteration near the flow tops. Similar interflow variation in physical properties has also been observed at Site 642 (e.g., Eldholm, Thiede, Taylor, et al., 1987; Planke, 1994) and Site 917 (e.g., Larsen, Saunders, Clift, et al., 1994; Planke and Cambray, in press).

Units 1 through 3, and possibly 4, 5, 6, and 13, are described as aa-type flow morphologies in the "Igneous Petrology" section (this chapter) whereas the remaining units (7–12) are described as either transitional or pahoehoe-type flows. These variations in morphology

correlate well with changes in the variability of measured physical properties (*P*-wave velocity, bulk density, and magnetic susceptibility) between flow units. In particular, there are larger variations in physical properties from within aa-type flows than in transitional or pahoehoe-type flows. Changes in *P*-wave velocity and bulk density are caused by changes in mineralogy and types and amounts of void space. Because flow types are described on the basis of vesicularity (void space), grain size, and texture, it is not surprising that *P*-wave velocity and bulk density correlate well with flow type morphologies. Thus, physical properties measurements can be helpful in designating flow boundaries and flow types.

REFERENCES

Barton, C., Moos, D., and Blangy, J.-P., 1989. Analysis of full waveform acoustic logging data at ODP Site 642—outer Vøring Plateau. *In* Eldholm, O., Thiede, J., Taylor, E., et al., *Proc. ODP, Sci. Results,* 104: College Station, TX (Ocean Drilling Program), 953–964.

Berggren, W.A., Kent, D.V., Swisher, C.C., III, and Aubry, M.-P., 1995. A revised Paleogene geochronology and chronostratigraphy. *In* Berggren, W.A., Kent, D.V., and Hardenbol, J. (Eds.), *Geochronology, Time Scales and Stratigraphic Correlation: Framework for an Historical Geology.* Spec. Publ.—Soc. Econ. Paleontol. Mineral., 54:129–212.

Birch, F., 1961. The velocity of compressional waves in rocks to 10 kilobars, 2. *J. Geophys. Res.,* 66:2199–2224.

Carlson, R.L., and Gangi, A.F., 1985. Effect of cracks on the pressure dependence of P-wave velocities in crystalline rocks. *J. Geophys. Res.,* 90:8675-8684.

Cheng, C.H., and Toksöz, M.N., 1979. Inversion of seismic velocities for the pore aspect ratio spectrum of a rock. *J. Geophys. Res.,* 84:7533–7543.

Delius, H., Buecker, C., and Wohlenberg, J., in press. Basaltic lava flows and volcaniclastic sediments and their significant log responses. In *Scientific Drilling:* Berlin (Springer).

Eldholm, O., Thiede, J., Taylor, E., et al., 1987. *Proc. ODP, Init. Repts.,* 104: College Station, TX (Ocean Drilling Program).

Fitton, J.G., Saunders, A.D., Larsen, L.M., Hardarson, B.S., and Norry, M.J., in press. Volcanic rocks from the East Greenland Margin at 63°N: composition, petrogenesis, and mantle sources. *In* Saunders, A.D., Larsen, H.C., Clift, P.D., and Wise, S.W., Jr. (Eds.), *Proc. ODP, Sci. Results,* 152: College Station, TX (Ocean Drilling Program).

Larsen, H.C., Saunders, A.D., Clift, P.D., et al., 1994. *Proc. ODP, Init. Repts.,* 152: College Station, TX (Ocean Drilling Program).

LeHuray, A.P., 1989. Native copper in ODP Site 642 tholeiites. *In* Eldholm, O., Thiede, J., Taylor, E., et al., *Proc. ODP, Sci. Results,* 104: College Station, TX (Ocean Drilling Program), 411–417.

Planke, S., 1994. Geophysical response of flood basalts from analysis of wireline logs: Ocean Drilling Program Site 642, Vøring volcanic margin. *J. Geophys. Res.,* 99:9279–9296.

Planke, S., and Cambray, H., in press. Seismic characteristics of subaerial flood basalts from wireline logging, ODP Hole 917A. *In* Saunders, A.D., Larson, H.C., Clift, P.D., and Wise, S.W., Jr. (Eds.), *Proc. ODP, Sci. Results,* 152: College Station, TX (Ocean Drilling Program).

Shipboard Scientific Party, 1994. Site 915. *In* Larsen, H.C., Saunders, A.D., Clift, P.D., et al., *Proc. ODP, Init. Repts.,* 152: College Station, TX (Ocean Drilling Program), 73–87.

Sinton, C.W., and Duncan, R.A., in press. $^{40}Ar/^{39}Ar$ ages of lavas from the southeast Greenland margin, ODP Leg 152, and the Rockall Plateau, DSDP Leg 81. *In* Saunders, A.D., Larsen, H.C., Clift, P.D., and Wise, S.W., Jr. (Eds.), *Proc. ODP, Sci. Results,* 152: College Station, TX (Ocean Drilling Program).

Sinton, C.W., Larsen, H.C., and Duncan, R.A., 1994. The timing of the volcanism at the southeast Greenland Margin, ODP Leg 152. *Eos,* 75:607.

Ms 163IR-105

NOTE: For all sites drilled, core-description forms ("barrel sheets") and core photographs can be found in Section 3, beginning on page 71. Thin-section data can be found in Section 4, beginning on page 253. See Table of Contents for material contained on CD-ROM.

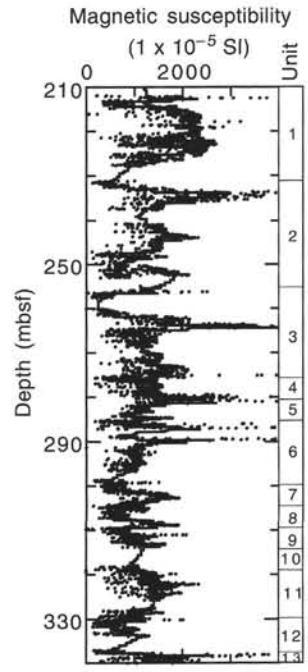

Figure 26. Magnetic susceptibility vs. depth for Hole 990A. Note the higher susceptibility values in the thick igneous Units 1, 2, 3, and 6. The points reflect raw data; the line represents a 15-point running average. Magnetic susceptibility was measured directly on split core sections using the MST.